Charles University in Prague
Faculty of Science

Department of Physical and Macromolecular Chemistry

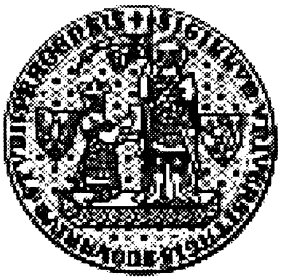

Application of Modern Fluorescence Techniques for Studies of Nano-organized Systems (Polymeric Micelles and Lipid Membranes)

Jana Humpolíčková

Supervisor:
Prof. RNDr. Karel Procházka, DrSc.

Consultant:
Doc. Dr. Martin Hof

PhD thesis

Prague 2006

The thesis was accomplished at the Department of Physical and Macromolecular chemistry at the Faculty of Science of the Charles University. My supervisor was prof. RNDr. Karel Procházka, DrSc. and the consultant was Doc. Dr. Martin Hof. Most of the fluorescent experiments were done at the J. Heyrovský Institute of Physical Chemistry of the Academy of Sciences of the Czech Republic. The measurements in cells were performed at the Department of Chemistry at the Katholieke Universiteit Leuven in Belgium.

I declare that I have elaborated the thesis on my own. If another already published results are used, they are included in the list of references. I agree with lending the thesis to anyone who may be interested.

Prague, 27. 6. 2006

Acknowledgement

At first, I would like to gratefully acknowledge everybody who has contributed to this work and who I can hardly imagine this work could be accomplished without. Particularly, I would like to thank to:

- My supervisor Karel Procházka for introducing me into the field of polymer science.
- Martin Hof for giving me an insight into the solvent relaxation method and fluorescence correlation spectroscopy and especially, for the kind human attitude to everybody in the lab.
- My colleagues from the Lab of Specialty Polymers, Mirek Štěpánek and Pavel Matějíček for all the expertise in the light scattering techniques and in the atomic force microscopy.
- My colleagues from the Martin Hof`s group, Aleš Benda for all the "know how" considering FCS and for his readiness to share it and Jan Sýkora for all the fun that arrised during the solvent relaxation and cellular measurements.
- Yves Engelborghs for allowing me to take part in the nice Czech-Belgium bilateral project focused on the research of Oligodendrocytes, Ellen Gielen and Veronika Fagulová for a friendly atmosphere around the confocal microscope in Leuven.
- All the colleagues who are not explicitly named for fruitful discussions and good time.

At last, but not least, I would like to thank to my parents for a patient and kind support.

List of Publications

[1] Humpolickova, J., K. Prochazka, and M. Hof. 2003. Octadecylrhodamine B as a specific micelle-binding fluorescent tag for fluorescence correlation spectroscopy studies of amphiphilic water-soluble block copolymer micelles. Spectroscopic behavior in aqueous media. *Collection of Czechoslovak Chemical Communications* 68(11):2105-2119.

[2] Humpolickova, J., K. Prochazka, M. Hof, Z. Tuzar, and M. Spirkova. 2003. Fluorescence correlation spectroscopy using octadecylrhodamine B as a specific micelle-binding fluorescent tag: Light scattering and tapping mode atomic force microscopy studies of amphiphilic water-soluble block copolymer micelles. *Langmuir* 19(10):4111-4119.

[3] Humpolickova, J., M. Stepanek, K. Prochazka, and M. Hof. 2005. Solvent relaxation study of pH-dependent hydration of poly(oxyethylene) shells in polystyrene-block-poly(2-vinylpyridine)-block-poly(oxyethylene) micelles in aqueous solutions. *J. Phys. Chem. A* 109(48):10803-10812.

[4] Humpolickova, J., E. Gielen, A. Benda, V. Fagulova, J. Vercammen, M. vandeVen, M. Hof, M. Ameloot, and Y. Engelborghs. 2006. Probing microheterogeneities within cellular membranes by Z-scanning fluorescence correlation spectroscopy. *Biophys. J.* in press.

[5] Matejicek, P., J. Humpolickova, K. Prochazka, Z. Tuzar, M. Spirkova, M. Hof, and S.E. Webber. 2003. Hybrid block copolymer micelles with partly hydrophobically modified polyelectrolyte shells in polar and aqueous media: Experimental study using fluorescence correlation spectroscopy, time-resolved fluorescence, light scattering, and atomic force microscopy. *J. Phys. Chem. B* 107(32):8232-8240.

[6] Stepanek, M., J. Humpolickova, K. Prochazka, M. Hof, Z. Tuzar, M. Spirkova, and T. Wolff. 2003. Light scattering, atomic force microscopy and fluorescence correlation spectroscopy studies of polystyrene-block-poly(2-vinylpyridine)-block-poly(ethylene oxide) micelles. *Collection of Czechoslovak Chemical Communications* 68(11):2120-2138.

[7] Matejicek, P., K. Podhajecka, J. Humpolickova, F. Uhlik, K. Jelinek, Z. Limpouchova, K. Prochazka, and M. Spirkova. 2004. Polyelectrolyte behavior of polystyrene-block-poly(methacrylic acid) micelles in aqueous solutions at low ionic strength. *Macromolecules* 37(26):10141-10154.

[8] Stepanek, M., P. Matejicek, J. Humpolickova, J. Havrankova, K. Podhajecka, M. Spirkova, Z. Tuzar, C. Tsitsilianis, and K. Prochazka. 2005. New insights on the solution behavior and self-assembly of polystyrene/poly(2-vinylpyridine) 'hairy' heteroarm star copolymers with highly asymmetric arms in polar organic and aqueous media. *Polymer* 46(23):10493-10505.

[9] Stepanek, M., P. Matejicek, J. Humpolickova, and K. Prochazka. 2005. Reversible aggregation of polystyrene-block-poly(2-vinylpyridine)-block-poly(ethylene oxide) block copolymer micelles in acidic aqueous solutions. *Langmuir* 21(23):10783-10790.

[10] Gielen, E., J. Vercammen, J. Sykora, J. Humpolickova, M. vandeVen, A. Benda, N. Hellings, M. Hof, Y. Engelborghs, P. Steels, and M. Ameloot. 2005. Diffusion of sphingomyelin and myelin oligodendrocyte glycoprotein in the membrane of OLN-93 oligodendroglial cells studied by fluorescence correlation spectroscopy. *Comptes Rendus Biologies* 328(12):1057-1064.

List of abbreviations

ACF	autocorrelation function
AFM	atomic force microscopy
CPM	counts per molecule
DiD	1,1′-dioctadecyl-3,3,3′,3′-tetramethylindodicarbocyanine perchlorate
DOPC	Dioleoylphosphatidylcholin
DOPS	Dioleoylphosphatidylserin
DRM	detergent resistant membrane
FCS	fluorescence correlation spectroscopy
FWHM	Full width in half maximum
GUV	giant unilamellar vesicles
IRF	instrument response function
Laurdan	6-lauroyl-2-dimethylaminonaphthalene
OLG	Oligodendrocytes
ORB	Octadecylrhodamine B
Patman	6-hexadecanoyl-2-(((2-(trimethylammonium)ethyl)methyl)-amino)naphthalene chloride
PMA	poly(methacrylic acid)
POE	poly(oxyethylene)
PS	Polystyrene
PS-PMA	polystyrene-*block*-poly(methacrylic acid)
PS-POE	polystyrene-*block*-poly(oxyethylene)
PS-PVP	polystyrene-*block*-poly(2-vinylpyridine)
PS-PVP-POE	polystyrene-*block*-poly(2-vinylpyridine)-*block*-poly(oxyethylene)
PVP	poly(2-vinylpyridine)
QELS	quasielastic light scattering
SLS	Static light scattering
SPB	supported phospholipid bilayer
TCSPC	time-correlated single photon counting
TRES	time-resolved emition spectra

Content

Introduction

Fluorescence and phosphorescence phenomena have been known for centuries, they are mentioned already in Chinese books from 1500 B.C. Scientific investigation, however, goes back to the very beginning of the 17th century when the famous Bolognian stone was accidentally discovered by a shoemaker and when later, a blue reflected and a yellow transmitted light was observed from the wood extract of *Lignum Nephriticum*. During the course of time, the phenomena became well understood and widely used. Most of common users of fluorescence techniques may nowadays think that all important questions dealing with fluorescence have been already answered and therefore they might not be aware that a huge development of fluorescence techniques still continues.

The advantage of fluorescence is that it is very specific because a relatively limited number of species exhibits this phenomenon in the visible spectral region. This causes that the signal from fluorescent probes is not usually affected by species that are to be visualized and by other species present in the system. Moreover, the photophysics of mostly used fluorophores is known and the properties of emitted light can serve as a source of information on the fluorescently labeled system of interest. This is very useful especially if complex systems are to be studied and thus fluorescent techniques are common tools in biochemistry and molecular biology.

The aim of this thesis is to introduce and optimize two newer fluorescent techniques for studying nanostructured systems. Even though these techniques have been already well established, they have been only little used in polymer science and still are to be developed in order to find new applications. The fluorescence techniques that are presented here are the relaxation of solvent and the fluorescence correlation spectroscopy (FCS).

The thesis is divided into four chapters. Since the majority of the work was done on the systems of block copolymer micelles, the very first part deals with micelles and gives a brief overview of two common benchmark techniques that were used in order to get more complex insight in the general behavior and a comparison with the fluorescence approach.

The second part of the thesis deals with the solvent relaxation, which has been so far used mainly in the biomembrane research. The chapter explains how the method works and shows an example of the triblock copolymer micelles where the experiments give an idea of the hydration of the polymer chains in the shell.

In the third and fourth part, two application of the fluorescence correlation spectroscopy are discussed. The first one concerns benefits of the FCS for aqueous solution of polymer micelles and compares the method with the static and dynamic light scattering. The second one aims at totally different system where FCS can be utilized and where scattering methods would be of no use. It deals with the membrane dynamics of living cells where lateral diffusion was studied in order to get detailed information on the membrane organization.

Even though the micellar solutions and living cells are nearly at the opposite ends of the spectrum of the scientific interest, the methods introduced in the thesis describe principles that are more or less general and applicable in both the cases.

Chapter I

Block Copolymer Micelles and Standard Benchmark Techniques

The first chapter brings a brief overview on block copolymer micelles that have been a subject of numerous studies in the Laboratory of Specialty Polymers at the Department of Physical and Macromolecular Chemistry for a long time.[1-5] *Since the following chapters deal with new techniques suitable for solving important questions concerning the micellar systems, this introduction describes also two standard benchmark techniques often used in polymer research: static and quasielastic light scattering and atomic force microscopy. The comparison of results of new and benchmark techniques will be given in the following chapters.*

1.1 Water soluble block copolymer micelles

Block copolymer micelles are nanoparticles formed by block copolymers with at least one block that is soluble and one that is insoluble in a given, so called selective solvent.[6-9] Provided the selective solvent is water, the micelle consists of the hydrophobic core and the hydrophilic shell.

Since in all studies included in this thesis, the core was formed either by polystyrene or poly(2-vinylpyridine) that are both insoluble in water, the micelles had to be prepared indirectly, i.e., by dissolving in the mixture rich in an organic solvent, mostly 1,4-dioaxane, which is a good solvent for hydrophobic blocks. During a consequent stepwise dialysis, the remaining organic solvent was removed and the core of the micelles got into the "kinetically frozen" state, which means that there was no exchange of polymer chains among micelles. This was proved by ultracentrifugation[10] and fluorescence experiments.[11] The core of the micelles is similar to the bulk polymer below the glass transition temperature.

The dialysis starts at the composition when all the blocks are in a thermodynamically good solvent. When the selective solvent is added, the anomalous micelles are usually formed. They are known to be rather polydisperse and unstable[12].

With increasing amount of the selective solvent, the regular micelization occurs. The micelles are in equilibrium with single polymer chains. The association number increases with amount of the selective solvent and eventually, the equilibrium gets to the kinetically frozen state with no free polymer in the solution.

If the amount of the selective solvent is suddenly increased, the equilibrium freezes at once, i.e., it is quenched and the association number stays unchanged.[13-15]

A typical polymer micelle consists of a compact core and the hydrophilic shell. If the shell is formed by polyelectrolyte, the effects related to changes in pH and ionic strength can be observed. In the case of a strong electrolyte, the hydrophilic chains are fairly stretched at low ionic strength. With increasing ionic strength, the micellar shell becomes more compact due to electrostatic screening.

The behavior becomes more complex in the case of weak polyelectrolytes. It has been shown that segments of the polyelectrolyte do not behave equally in the radial direction from the core as their microenvironment changes significantly between the core and the outer side of the shell. This causes a partial collapse of parts of polyelectrolyte chains close to the core and a pronounce dependence of the segment density and the electrostatic potential on the radial distance (see Schematics I).[16, 17] Apart from the ionic strength effects, a strong influence of pH can be observed. It has been shown that whereas the outer part of the micellar shell reflects the pH changes immediately, the segments close to the core are less accessible and thus the kinetics is considerably slower.[1]

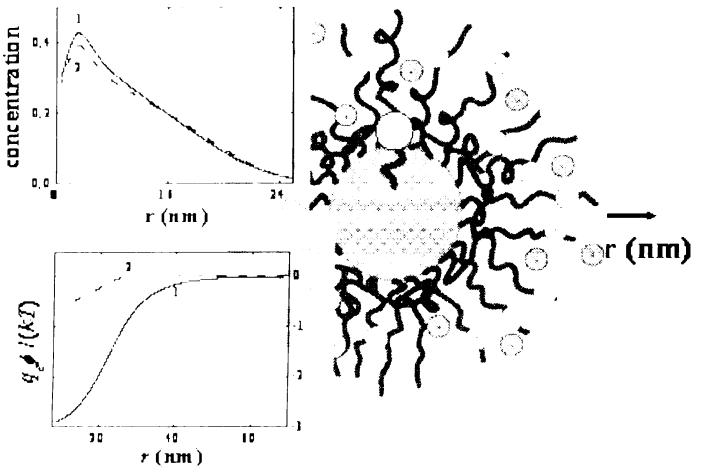

Schematics 1. Diblock copolymer (block polyelectrolyte) micelle with an embedded fluorescent dye, patman for instance (gray sphere with tail) – the schematics shows the gradient in micellar properties: the electrostatic potential and segment concentration decrease in the radial direction. Lower inset: The reduced electrostatic potential, i.e., $q_e\phi(r)/kT$, where q_e is the elementary charge $\phi(r)$ the electrostatic potential, k the Boltzmann constant and T temperature, as a function of the distance from the micellar center, r, for dilute aqueous solution of micelles at pH close to the effective dissociation constant of the weak polyelectrolyte, pK_A, and I = 0.001 and 0.1, the full curve 1′and dashed curve 2′, respectively.[18] Upper inset: Curves 1 and 2 show corresponding concentration profiles of segments of polystyrene-*block*-poly(methacrylic acid) (PMA) in the shell. The schematics is based on results of our earlier studies for PMA micelles.[22] For the weak polybase such as PVP, the curves are schematically the same only the sign of the potential is opposite. The simulated density profile is not monotonous and rises slightly at short distances from the PS core. This is an artifact of the simulation model, which assumes that the surface of the PS core is absolutely impenetrable for the shell-forming chains. In real micelles, the uncharged parts of the shell-forming chains are slightly intermixed with PS chains at the interfacial region and the shell density decreases monotonously in the radial direction.

1.2 Standard benchmark techniques used in the micellar research

1.2.1 Light scattering

Since the polymer micelles are strong scatterers, static and quasielastic light scattering techniques are standard tools for studying their solutions.

In the static light scattering (SLS), the angular and concentration dependences of scattered light intensity are measured and characterized by the excess Rayleigh ratio:

$$\Delta R(q,c) = \frac{I(q,c) - I(q,0)}{I_0} r^2, \qquad (1)$$

where I_0 is the intensity of the initial light, r is the distance between the scatterer and the detector, q is the scattering vector: $q = |\vec{q}| = |\vec{k} - \vec{k}_s| = \frac{4\pi n_0}{\lambda} \sin\frac{\vartheta}{2}$, $\vec{k}$ and $\vec{k}_s$ are the wave vectors of the initial and the scattered light in the particular direction, respectively, ϑ is the angle between $\vec{k}$ and $\vec{k}_s$.

If the particles are smaller than $\lambda/20$, the Rayleigh ratio is angularly independent and the light scattering data evaluated by the means of Zimm plots provide generally information on the weight averaged molar mass and the second osmotic virial coefficient only.

In the case of large particles (larger than $\lambda/20$), the light beams scattered at different parts of large particles interfere and the Rayleigh ratio becomes angularly dependent. The angular dependence provides information on the shape of particles that can be withdrawn from the angular dependence of the particle form factor: $P(q) = \frac{R(q)}{R(0)}$. In this case, the z-averaged radius of gyration can be evaluated.

Quasielastic light scattering (QELS) is based on the measurement of the autocorrelation function of fluctuations in the scattered light intensity:

$$g_2(\tau) = \frac{\lim_{T\to\infty} \int_0^T I(t) I(t+\tau) dt}{\langle I \rangle^2}. \qquad (2)$$

The function $g_2(\tau)$ is connected via the Siegert relation with the autocorrelation function $g_1(\tau)$ of electric field intensity $E(t)$ ($g_1(\tau) = \frac{\lim_{T\to\infty}\int_0^T E(t)E^*(t+\tau)dt}{\langle E \cdot E^* \rangle}$):

$$g_2(\tau) = 1 + \beta g_1^2(\tau), \tag{3}$$

where β is the apparatus constant. For slightly polydisperse systems, the function $g_1(\tau)$ can be fitted by the means of cumulants:

$$\ln g_1(\tau) = \ln A - \Gamma\tau + \frac{\mu_2}{2}\tau^2 - \frac{\mu_3}{6}\tau^3 + \ldots + (-1)^n \frac{\mu_n}{n!}\tau^n. \tag{4}$$

A is the amplitude, Γ is the relaxation rate, μ_i are so called cumulants. For highly polydisperse systems, the inverse Laplace transform gives the spectrum of relaxation times τ or relaxation rates Γ, which are related to the diffusion coefficient D of the scattering particles $\Gamma = Dq^2$, via relations:

$$g_{1(1)}(t) = \int_0^\infty \tau A(\tau) e^{-t/\tau} d\ln\tau, \tag{5}$$

$$g_{1(1)}(t) = \int_0^\infty G(\Gamma) e^{-\Gamma t} d\Gamma. \tag{6}$$

1.2.2 Atomic force microscopy

Atomic force microscopy (AFM) is nowadays one of often used techniques in polymer studies.[19, 20] It directly vizualizes the surface of interest. Thus, if aqueus solutions of polymer micelles are to be studied, the sample has to be first deposited on the surface. The conditions are, of course, different at the surface and in the solution and the macromolecules can change their size, conformation and other properties. Therefore results of AFM measurements have to be confirmed by other techniques.

The AFM method was developed by Binnig, Quate and Gerber in 1986.[21] It monitores the interaction between a sharp tip of the cantilever during surface scanning. Three different modes are commonly used in AFM. It is (i) a contact mode, (ii) a non-contact mode and (iii) a tapping mode. In all the three cases, the position of the cantilever is followed by observing reflection of the laser beam from the cantilever. The

movement of the cantilever is sensitively controled by changing of electric voltage on the piazoelectric tube.

For the study of adsorbed polymer micelles and films, the most convenient mode seems to be the tapping mode as it minimizes the direct contact of the cantilever with the surface. At this mode, the cantilever oscilates with its resonance frequency and amplitude typically between 20 and 100 nm. The tip is in a contact with the surface through the adsorbed liquid layer above the sample merely close to the bottom turning point. Since the amplitude is kept constant as well as the interaction force between the sample and the cantilever, it is the vertical position of the scanner what changes.

In order to optimize the imaging, the surfaces with the lowest roughness are the most convenient. One of the best materials for our studies seems to be mica, which due to its layered structure, is flat on the atomic level. It is generaly recognized that the highly hydrophilic mica surface is negatively charched and thus very good for binding polycations.[22-24] However, the freshly prepared mica surface is full of small positive counterions and thus binds polyinons as well.

Chapter II

Solvent Relaxation in Block Copolymer Micelles

The solvent relaxation technique has been exhibited as a useful tool for membrane studies for more than one decade already.[25-36] *It brings a good insight into the hydration of lipids at different depths of membranes in large unilamellar vesicles and shows how this can be affected by lipid composition and temperature. If the so called „time-zero" is properly estimated and the time evolution of spectral halfwidth is monitored, the information on the amount of water and its mobility becomes reliable and very convincing.*

For the aqueous solutions of polymer micelles, the solvent relaxation technique was never properly and systematically used, even though there are questions that can be solved exclusively by this method. This chapter shows that the level of hydration at the particular position in the micelles can be well monitored by the solvent relaxation approach. The attention is mainly focused on the solvation of poly(oxyethylene), which has very favourable geometrical prerequisites to be well hydrated in water.[37] *In the shell of polystyrene-block-poly(2-vinylpyridine)-block-polyoxyethylene) micelles, however, the hydration seems to be pretty different and to depend on the organization of the whole micelle (pH changes or aggregation for instance). The results obtained from solvent relaxation were compared with results from other techniques and summarized in the enclosed publication.*[38]

2.1 Fluorescent solvent relaxation

2.1.1 Basic principles

Solvent relaxation is a fluorescent technique that expoits large dipole moment changes of certain fluorophores upon excitation. The orientation of polar solvent molecules (possesing a dipol moment and solvating the fluorophore) minimizes the overall energy of the system. When the fluorophore absorbs the excitation light, the dipole moment changes on the femtosecond time scale. The dipoles of solvent molecules tend to minimize the solvation energy and start to reorient, however, do not

follow the fast change immediately. Depending on the microviscosity of the fluorophore microenvironment, the so called solvent relaxation occurs from several tens of picoseconds up to several nanoseconds. Since the emission of photons is a nanosecond process, the time resolved red-shift of the emission spectra can be observed. (See Schematics II)

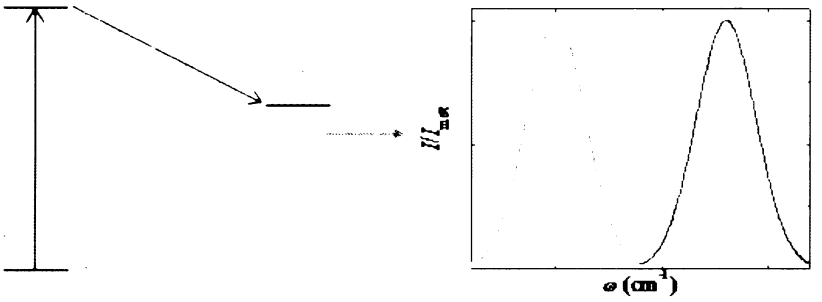

Schematics II. The dipol moment changes upon excitation and the solvent molecules start to reorient in order to minimize the overall energy. This causes the time-resolved red shift of the fluorescence spectra.

2.1.2 Read-out parameters

The overall difference between the emission spectra immediately after the excitation $\nu(0)$ and in the fully relaxed state $\nu(\infty)$, the overall Stokes shift $\Delta\nu = \nu(0) - \nu(\infty)$, reflexes the polarity of the fluorophore microevnironment. If the relaxation is fast (in the subpicosecond time range), which is in the case of flourophores dissolved in non-viscous solvents at ambient temperatures, the observed steady-state emission goes mainly from the relaxed state and the position of the steady-state emition maximum reffers to the polarity of bulk solvents.

If the friction forces in the microenvironment of the probe increase, the relaxation process slows down and the rate of the relaxation response relates to the microviscosity. The kinetics of the relaxation can be described by the correlation function $C(t)$:

$$C(t) = \frac{\nu(t) - \nu(\infty)}{\nu(0) - \nu(\infty)}. \qquad (7)$$

To quantify the rate, it is suitable to define the integral relaxation time τ:

$$\tau = \int_0^{\infty} C(t)dt \tag{8}$$

that has been shown to be a reasonable measure of the microviscosity of the probe. [39-41]

2.1.3 Time-zero estimation

To be able to evaluate the overall Stokes shift, the emission spectrum at time-zero, i.e., immediately upon the excitation prior any relaxation process, is needed. The method allowing for calculating the time-zero spectrum was suggested by Fee and Maroncelli[42] and is based on the following assumptions: i) the broadening of the absorption spectra of the particular dye in any solvent results from the effect of inhomogeneous distribution of solvent environments (spectral shifts) on the intrinsic vibronic line shape $g(\nu)$, which is assumed to be solvent independent. ii) The distribution function of solvent-induced shifts is supposed to be Gaussian shaped:

$$p(\delta) \quad \frac{1}{\sqrt{2\pi\sigma}} \exp\left(\frac{-(\delta - \delta_0)^2}{2\sigma^2} \right). \tag{9}$$

The absorption spectra in a solvent can be thus expressed as follows:

$$A_p(\nu) \propto \nu \int g(\nu - \delta) p(\delta) d\delta . \tag{10}$$

Similarly, the emission spectrum at the time zero is given:

$$F_p(\nu, t = 0, \nu_{ex}) \propto \nu^3 \int g(\nu_{ex} - \delta) p(\delta) f(\nu - \delta) d\delta . \tag{11}$$

In order to reconstruct the time zero emission spectra, three functions are needed: vibronic line shape $g(\nu)$, emission line shape $f(\nu)$ and the parameters of the Gaussian shaped spectral shifts distribution. The functions $g(\nu)$ and $f(\nu)$ are solvent independent and can be obtained from the absorption and emission spectra of the particular dye in a non-polar solvent, where no solvent relaxation is supposed to occur:

$$g(\nu) \propto \nu^{-1} A_{ref}(\nu) \tag{12}$$

and

$$f(\nu) \propto \nu^{-3} F_{ref}(\nu). \tag{13}$$

The parameters of the Gaussian distribution δ_0 and σ are detremined by iterative fitting of the polar absorption spectrum (equation (10)).

2.1.4 Halfwidth of TRES

The discussed time-zero estimation provides us with infromation where the relaxation process starts on the energy (i.e., frequency) scale and cosequently, what fraction of the overall solvent relaxation can be seen within the time window of the experiment. Qualitative information on the extent of the observed process can be also obtained from the time-evolution of the half width of the emission spectrum.

Experiments carried out in supercooled liquids[43] and in phospholipid bilayers[25, 34] have shown that the halfwidth passes a maximum, which is in agreement with the idea of non-uniform spatial distribution of solvent response times.[43, 44] It has been shown that in homogeneous systems of low-molar-mass molecules, the halfwidth always decays monotonously. In a spatially inhomogeneous system (it applies also to inhomogeneity on the nanometer length-scale), the relaxation behavior is different. Since the properties of the system vary in space, individual fluorophores distributed in the system are not equivalent and their solvent shells respond with different rates to the local electric field. This inhomogeneity gives rise to a new phenomenon, which reflects the time distribution of phases of relaxations of individual solvation shells during the relaxation. The observed transient inhomogeneity increases significantly and the time-dependence of the observed halfwidth passes a pronounced maximum.

The above described time-evolution enables us to decide whether the experimental time-window is broad enough for the entire relaxation. If only the decrease is observed, the relaxation is beyond the experimental resolution, in the opposite case, if only the increase appears, the deexcitation is faster than the relaxation.

2.1.5 Time-correlated single photon counting and generating of TRES

The time-resolved emission spectra (TRES) are usually reconstructed from directly measured fluorescence decays. The decays are collected by the method of time-correlated single photon counting (TCSPC).[45-47] The resolution of the experimental setup is in the subpicosecond time-range. The measured data are fitted with an exponential decay:

$$I(t) = A + \sum_{i=1}^{n} \alpha_i \exp\left(-\frac{t}{\tau_i}\right), \qquad (14)$$

A is a correction to the background, α_i are the amplitudes and τ_i stands for decay times. The fit has to be convoluted with the instrument response function (IRF) and the parameters of the fit are obtained iteratively by minimizing χ^2:

$$\chi^2 = \frac{1}{v}\sum_{i=1}^{N}\left(\frac{R(t_i)-R_c(t_i)}{\sigma_i}\right)^2 . \tag{15}$$

v stands for the number of degrees of freedom, $R(t_i)$ are the measured data, $R_c(t_i)$ is the fitted function convoluted with IRF and σ_i is the standard deviation.

TRES $S(\lambda,t)$ are calculated from the decays by the method called spectral reconstruction. It requires to measure the steady state spectrum $S_0(\lambda)$ and the fluorescence decays $D(t,\lambda)$ at various wavelengths that span the steady state emission spectra that is needed for the normalization of the decays:

$$S(\lambda,t) = \frac{D(t,\lambda)\times S_0(\lambda)}{\int_0 D(t,\lambda)dt}. \tag{16}$$

In order to get the time-dependence of the spectral maximum and the time evolution of the full width in half maximum (FWHM), TRES are at first recalculated to the wavenumbers and consequently fitted with a log-normal function:

$$\begin{aligned} F(\nu,t) &= h\exp\left[-\ln(2)\left\{\ln\left(\frac{(1+\alpha)}{\gamma}\right)\right\}^2\right], \text{ for } \alpha > -1 \\ F(\nu,t) &= 0, \qquad\qquad \text{for } \alpha \le -1 \end{aligned} \tag{17}$$

where

$$\alpha = \frac{2\gamma(\nu-\nu_p)}{\Lambda}. \tag{18}$$

h is the peak height, ν_p is the peak position, γ is the asymmetry parameter and Λ is the width parameter which both are related to FWHM:

$$\mathrm{FWHM}(t) = \Lambda(t)\left(\frac{\sinh(\gamma(t))}{\gamma(t)}\right). \tag{19}$$

2.2 Solvent relaxation in block copolymer micelles

2.2.1 Diblock copolymer micelles

It has been shown that the solvent relaxation is a good tool to monitor the micropolarity and microviscosity of the fluorophore. The first question that has to be answered concerns the time scale of the solvent relaxation in the shells of block copolymer micelles. In the bulk water, the rearrangement of so called "free" water molecules occurs in the subpicosecond time range, which is beyond the resolution of the TCSPC experiment. In the micellar shell, however, water molecules form the hydration sphere of the units of polymer chains (so called "bound" water molecules) and thus their movement is considerably slowed down. Moreover, the rearrangement does not occur equally in all the three dimensions any more. It depends on the radial position in the shell similarly as all other properties do (see Schematics I).

In the case of water solutions of diblock copolymer micelles, several different solvent relaxation responses can be observed depending on where the fluorescent probe is located. Three fundamentally different solvent relaxation patterns reflecting the content of "free" and "bound" water molecules were observed in these three micellar systems:

a) Polystyren-*block*-poly(oxyethylen) micelles (PS-POE) labeled with Laurdan (see Chart I):

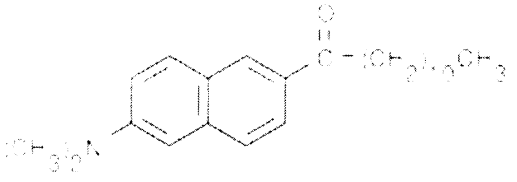

Chart I. Laurdan

Laurdan is a non-charged probe with 12-carbon long aliphatic chain, which causes that the dye is solubilized in the polystyrene core, where no water molecules are present. Thus, the relaxation is attained by rearrangement of polymer chains. The time-zero estimation suggests that we see only the very beginning of the process. The chain motion in the glassy polystyrene core is rather slow, which causes that the entire relaxation is not finished within the

lifetime of Laurdan. This can be observed both in the correlation function and the halfwidth behavior (see Fig. 1).

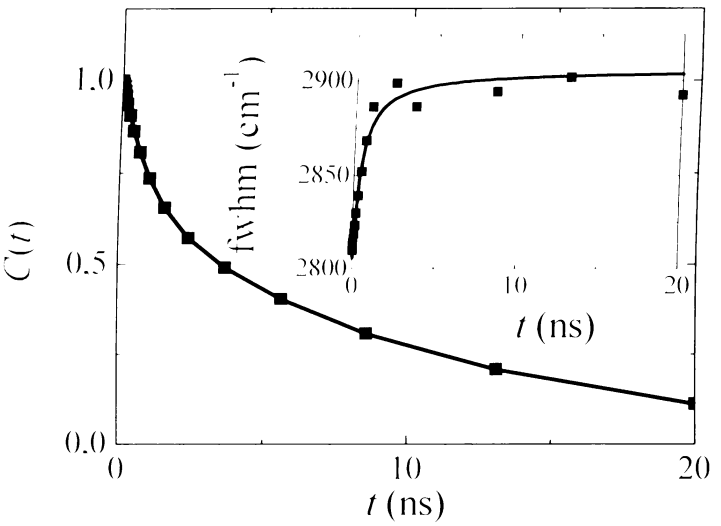

Figure 1. Time-resolved Stokes shift, $C(t)$, of laurdan in PS-POE micelles. Inset: Time-dependent halfwidth of time-resolved emission spectra of laurdan in PS-POE micelles.

b) Polystyren-*block*-poly(oxyethylen) micelles (PS-POE) labeled with Patman (see Chart II).

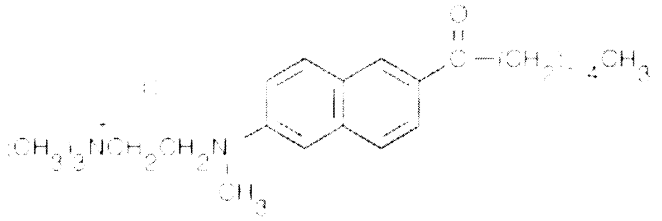

Chart II. Patman

Patman is an amphiphilic molecule, which has a 16-carbon long aliphatic chain, but in contrast to Laurdan, it also bears a positive charge. Thus, it is supposedly located at the core/shell interface. The time-zero estimation reveals that the beginning of the relaxation cannot be seen since it is beyond the resolution of the TCSPC experiment. This suggests that "free" water molecules already contribute to the rearrangement, but more than 60 % of the relaxation can be

still seen with the subnanosecond resolution. Moreover, the halfwidth expresses a clear maximum (see Fig. 2), which allows us to conclude that mainly "bound" water molecules are responsible for the relaxation at the core/shell interface.

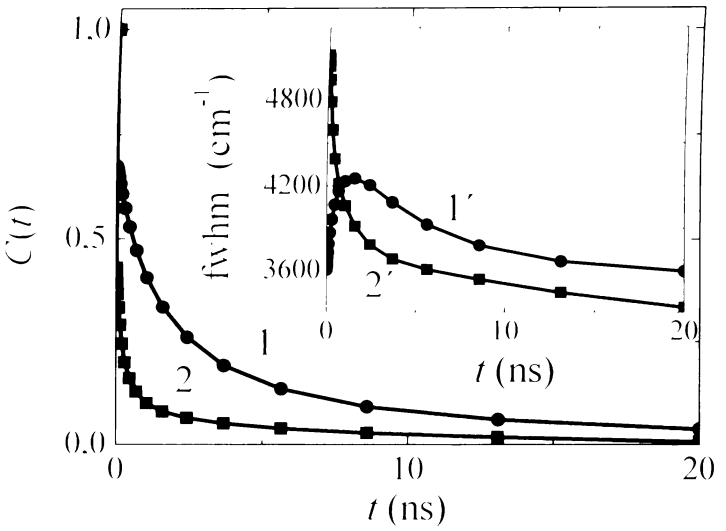

Figure 2. Time-resolved Stokes shift, $C(t)$, of patman in PS-POE micelles (curve 1) and PS-PVP micelles (curve 2). Inset: Time-dependent halfwidth of the time-resolved emission spectra of patman in PS-POE micelles (curve 1′) and in PS-PVP micelles (curve 2′).

c) Polystyren-*block*-poly(2-vinylpyridine) micelles (PS-PVP) labeled with Patman. In the acidic media at pH 2, the polyvinylpyridine chains are highly protonated and stretched to the solution due to the repulsion between electric charges. It has been shown that close to the core,[48] the polyvinylpyridine chains are less protonized and form collapsed domains, where Patman is supposed to be buried. In the PS-PVP micelles compared to the PS-POE micelles, there is more space among stretched polymer chains and thus, more water molecules are present close to the core. Therefore, the relaxation in PS-PVP micelles is faster. We can see slightly less than 50 % of the entire process, which is well confirmed by the fact that time-dependent halfwidth misses the maximum and merely decreases (see Fig. 2).

2.2.2 Triblock copolymer micelles

The above mentioned different solvent relaxation responses help us understand the pH-induced changes in the hydration of the PVP/POE interface of polystyrene-*block*-poly(2-vinylpyridine)-*block*-poly(oxyethylene) (PS-PVP-POE) micelles.

PS-PVP-POE micelles consist of a glassy polystyrene core, an inner poly(2-vinylpyridine) and an outer poly(oxyethylene) shell. The micelles were studied in the pH range from 1 to 4, where the protonation of the inner shell changes considerably. The Fig. 3a shows the degree of protonation in comparison with PS-PVP micelles. Obviously, the polyoxyethylene layer slightly suppresses the protonation at lower pH, however, it plays a significant role in suppressing changes in the hydrodynamic radius of PS-PVP-POE micelles compared with the PS-PVP micelles (see Fig. 3b).

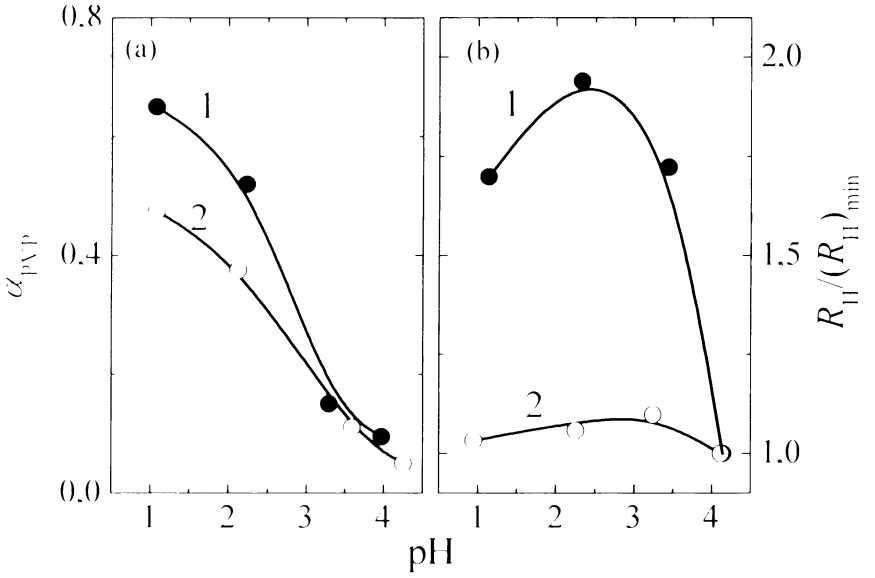

Figure 3. (a) Degree of protonization, α_{PVP}, of the PVP shell-forming blocks in PS-PVP (curve 1) and PS-PVP-POE (curve 2) micelles as a function of pH of the solution. (b) Relative hydrodynamic radius, $R_H/(R_H)_{min}$, of PS-PVP (curve 1) and PS-PVP-POE (curve 2) micelles as a function of pH of the solution. $(R_H)_{min}$ for PS-PVP and PS-PVP-POE micelles were 83 and 28 nm, respectively.

The PS-PVP-POE micelles were labeled with Patman, which is supposed to be located at the PVP/POE interface.[38] Thus the solvent relaxation probed by Patman visualizes hydration changes of poly(oxyethylene) close to the PVP/POE interface.

Surprisingly, even though the hydrodynamic radius of micelles does not almost change, the changes in the hydration of POE are substantial as the Fig. 4 shows.

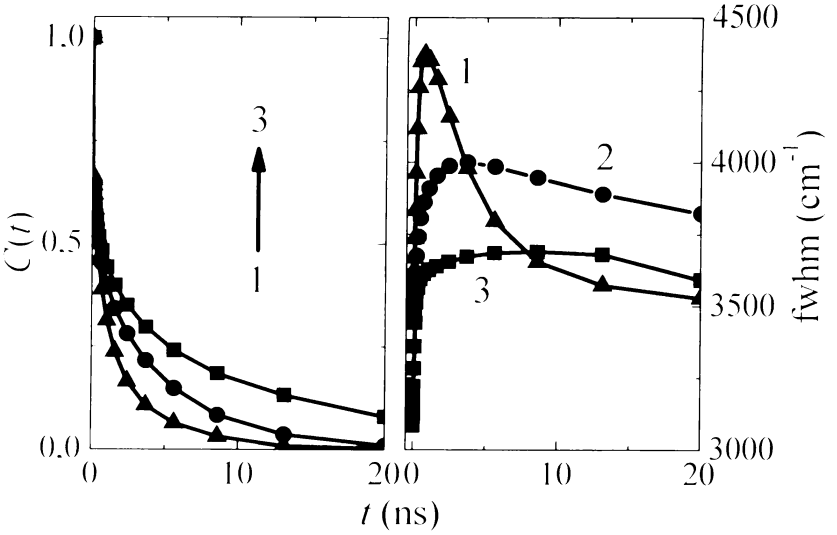

Figure 4. Left: Time-resolved Stokes shift, $C(t)$, of patman in PS-PVP-POE micelles at different pHs. pH 2 (curve 1), pH 3 (curve 2), pH 4 (curve 3). Right: Time-dependent halfwidths of the time-resolved emission spectra of patman in PS-PVP-POE micelles at pH 2 (curve 1), pH 3 (curve 2), pH 4 (curve 3).

At pH 4, similarly to the case of PS-POE micelles labeled with Laurdan, Patman does not "see" any water molecules, which is obvious from the correlation curve that cannot monitor the end of the process as well as from the halfwidth shape. With decreasing pH, the process speeds up, thus, a pronounced maximum appears in the halfwidth time-dependence and the integral relaxation time shortens. The amount of the unresolved relaxation increases with decreasing pH, which suggests that more and more "free" water molecules contribute to the entire rearrangement.

2.2.3 Aggregation of PS-PVP-POE micelles at low pH confirmed by solvent relaxation

The aforementioned experiment was carried out also at pH 1. In contrast to pH 2, where the reconstructed normalized TRES are monomodal and the relaxed states have the maximum at 21300 cm^{-1}, the TRES for pH 1 are bimodal. The Fig. 5 clearly reveals that in the totally relaxed state, there is merely a shoulder at 21300 cm^{-1} and the main maximum is at higher wavenumber. This suggests that Patman is

inhomogeneously distributed in individual PS-PVP-POE micelles in two domains differing significantly in polarity. The first localization corresponding to the higher Stokes shift is probably the same as at pH 2. The second localizaton with smaller Stokes shift belongs to a less polar and possibly even more rigid environment of the probe.

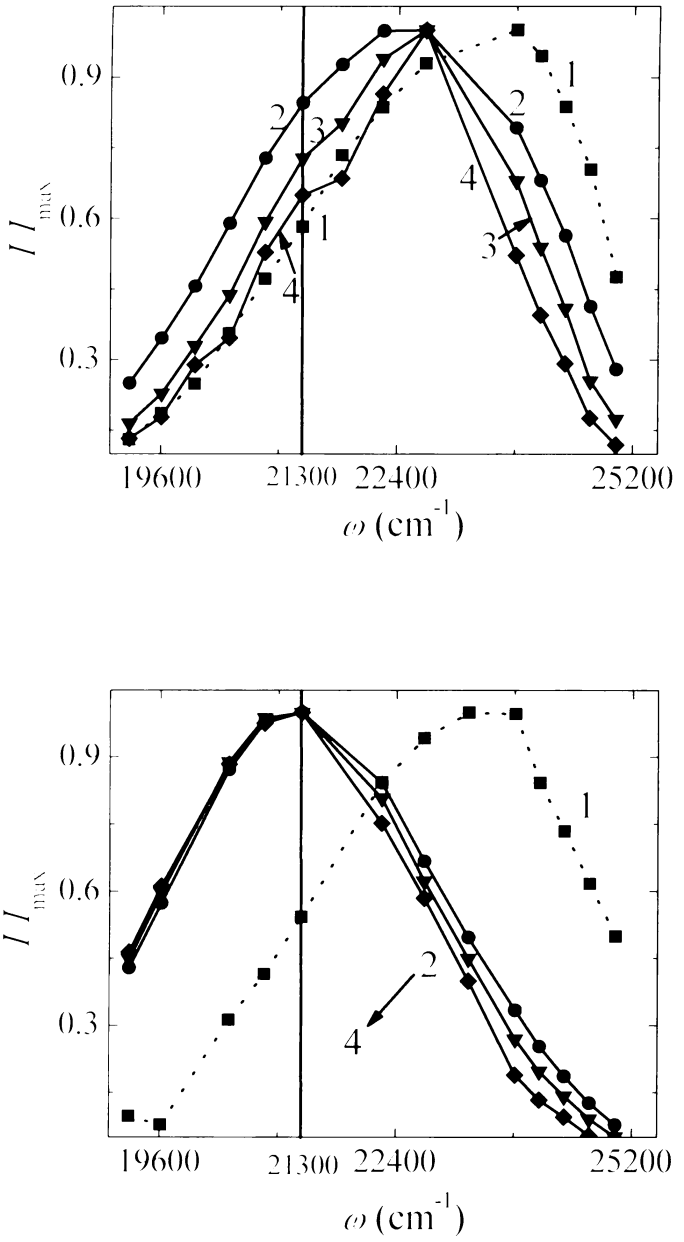

Figure 5a, 5b. Normalized time resolved emission spectra of patman in PS-PVP-POE micelles at pH 1 (Fig. 4a) and pH 2 (Fig. 4b) at "time zero" (curve 1), 1 ns (curve 2), 13 ns (curve 3) and 20 ns (curve 4) after the excitation.

Light scattering and atomic force microscopy studies have revealed[49] that the micelles show a strong tendency to aggregate at low pH. The micelles have a relatively short polystyrene block, thus the cores are not glassy. This causes that the individual chains can reorient and form transient "hemimicelles" that finally may stick together and from aggregates. The second position of Patman is thus supposed to be in the micellar aggregates.

Chapter III

Fluorescence Correlation Spectroscopy in Three Dimensions: Application in Polymer Micelles Research

The third chapter is devoted to a brief introduction in the fluorescence correlation spectroscopy (FCS) and its applications in three dimensions, i.e., in solutions. The method was established in seventies and found a lot of applications mainly in biochemical studies. It is a very suitable tool to study changes in diffusion, for instance during DNA condensation[50-53] *or protein – protein interaction.*[54, 55]

Since the studied biochemical problems are often complex and since there is no straightforward method for evaluation diffusion properties of labeled molecules based on fluorescence fluctuations, the results, even though convincing, are mostly interpreted merely on the qualitative level. Polymer micelles as relatively well defined and small particles can serve as good systems to investigate problems related with labeling or photophysics of the particular dye.

Based on FCS read-out parameters, the number-averaged molecular mass and hydrodynamic radius of micelles have been determined and discussed in comparison with results obtained from other established techniques. It turns out that FCS is a good complementary approach to light scattering, however, it has strong limitations that has to be taken into account. There are more details in the enclosed publications.[56, 57] *The method was further used to get a more complex insight in other studies of block copolymer micelles*[18, 49, 58-60]

3.1 Fluorescence correlation spectroscopy

3.1.1 Basic principles

Fluorescence correlation spectroscopy (FCS) is a relatively new technique which was introduced by Magde, Elson and Webb in 1972.[61] It is a microscopical technique that uses a confocal microscope to focus a laser beam, which than determines a working "cuvette". The fluorescence signal measured in the "cuvette" of the focused

volume size (1 fL), provided the concentration of fluorophores is in the nanomolar range, exhibits strong fluctuations. The fluctuations are not chaotic since the volume contains just units of fluorescent particles and they correlate with processes that cause the fluctuations, for instance Brownian motion, triplet formation or chemical reactions.[62-66]

Mathematical treatment of the fluctuating fluorescent intensity provides the autocorrelation function, which has to be fitted with an appropriate mathematical model that *a priori* assumes what processes are responsible for the fluctuations.

3.1.2 Experimental setup

The standard FCS setup is shown in the Schematics III. The laser radiation is reflected via a dichroic mirror (wavelength dependent beam splitter) into a water emersion objective with a high numerical aperture. The beam is focused into the sample that is placed at the working distance of the objective. Fluorescence signal as well as back reflected light, Rayleigh and Raman scattering is than gathered by the same objective and the red shifted fluorescence is transmitted through the same dichroic mirror and comes to the detector (avalanche photodiode).[67]

To increase the signal-to-noise ratio, i.e., to suppress the Raman scattering and the laser line that was not effectively enough filtered off, further emission filters are required. Furthermore, there is a pinhole in the image plane, which cut off all the photons that do not come from the focal region.

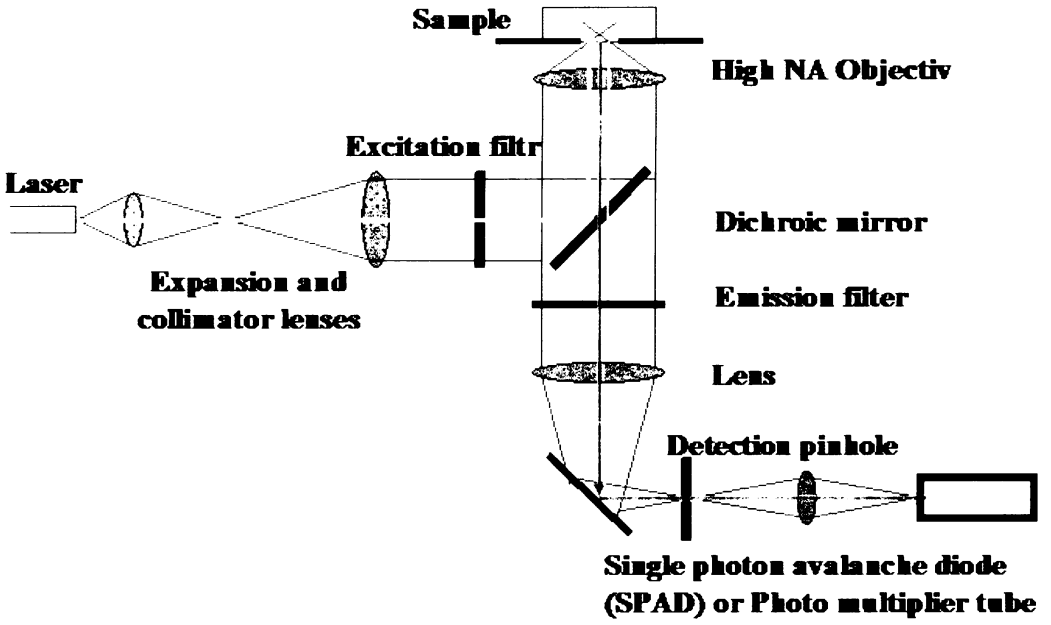

Schematics III. Schematic setup of the epifluorescence confocal microscope

3.1.3 Mathematical treatment of FCS data in three dimensions

The fluorescence fluctuations are treated via the intensity autocorrelation function $G(\tau)$:

$$G(\tau) = \frac{\langle F(t)F(t+\tau)\rangle}{\langle F(t)\rangle^2}. \tag{20}$$

The fluorescence intensity $F(t)$ can be written as the sum of the average intensity and the temporal fluctuation: $F(t) = \langle F(t)\rangle + \delta F(t)$, the autocorrelation function (ACF) can be than rewritten:

$$G(t) = 1 + \frac{\langle \delta F(t)\delta F(t+\tau)\rangle}{\langle F(t)\rangle^2}. \tag{21}$$

The fluctuations in intensity are determined by the spatial distribution of the excitation energy $I_{ex}(\boldsymbol{r})$, light-collection efficiency function of the setup (objective – pinhole alignment) $S(\boldsymbol{r})$ as a function of the position $\vec{r} = \{x, y, z\}$, the overall detection efficiency κ and the dynamics of the individual fluorophore $\delta(\sigma q C(\vec{r}, t))$, σ is the absorption cross section, q is the quantum yield, $C(\boldsymbol{r},t)$ is the local fluorophore concentration, that fluctuates mainly due to the Brownian motion.

Spatial distribution of the excitation energy together with collection efficiency function can be approximated by three-dimensional Gaussian function:

$$W(r) = \frac{I_{ex}(r)}{I_0} \cdot S(r) = \exp\left(-\frac{x^2 + y^2}{\omega_0^2}\right) \cdot \exp\left(-\frac{z^2}{z_0^2}\right), \tag{22}$$

where I_0 is the amplitude of the light intensity, ω_0 and z_0 are the halfwidth and the half of the focused volume height, respectively.

The rest of the parameters can be treated separately: $\eta = \kappa\sigma_{ex}I_0$, κ is the overall detection efficiency. The intensity fluctuation can be than written: $\delta F(t) = W(r)\delta(\eta C(r,t))$.

Provided η does not change with time, ACF is as follows:

$$G(t) = 1 + \frac{\iint W(r)W(r')\langle \delta C(r,t)\delta C(r',t+\tau)\rangle \mathrm{d}r\mathrm{d}r'}{\left(\langle C(t)\rangle \int W(r)\mathrm{d}r\right)^2}. \tag{23}$$

Considering only the presence of particles freely diffusing in all three dimensions, we get the following expression for the diffusion term:

$$\langle \delta C(r,t)\delta C(r',t+\tau)\rangle = \langle C(t)\rangle \frac{1}{(4\pi D\tau)^{3/2}} \exp\left(\frac{(r-r')^2}{4D\tau}\right). \tag{24}$$

Finally, we obtain the formula for the autocorrelation function for one freely diffusing particle:

$$G(\tau) = \frac{1}{N} \cdot \frac{1}{1+\frac{\tau}{\tau_D}} \cdot \frac{1}{\sqrt{1+\left(\frac{\omega_0}{z_0}\right)^2 \cdot \frac{\tau}{\tau_D}}}, \tag{25}$$

where N is the average number of particles in the focus volume, τ_D is the diffusion time, i.e., the average time the fluorescent molecule stays in the focused volume. It is related to the diffusion coefficient D as follows:

$$\tau_D = \frac{\omega_0^2}{4D}. \tag{26}$$

The assumption that the photophysics of the fluorophore does not change while the dye resides in the focused volume, unfortunately, does not hold for the most cases. The most common feature to be observed is the transition to the triplet state. The transition from the triplet state back to the ground state is forbidden from the quantum mechanical point of view and thus it is much slower. Consequently, fluorophores in the triplet states appear to be dark. This kind of "flickering" can be either directly added to

the formula for the autocorrelation curve, or as long as it occurs on much shorter time-scale than diffusion, it can be treated separately:[66]

$$G_{total}(\tau) = G_{motion}(\tau) G_{triplet}(\tau). \tag{27}$$

Finally, including the triplet formation term, the total autocorrelation function is given:

$$G(\tau) = \left(1 - T + T\exp\left(-\frac{\tau}{\tau_{triplet}}\right)\right)\frac{1}{N}\cdot\frac{1}{1+\frac{\tau}{\tau_D}}\cdot\frac{1}{\sqrt{1+\left(\frac{\omega_0}{z_0}\right)^2\cdot\frac{\tau}{\tau_D}}}. \tag{28}$$

T is the fraction of molecules in the triplet state, $\tau_{triplet}$ is the triplet constant.

In general, any process, considerably faster than diffusion, which might be described as switching between two states differing in the photophysical properties (cis-trans isomerization, for instance) can be treated similarly.

In the case of multiple species, the formula becomes rather complicated:

$$G(\tau) = \frac{1}{N_{total}}\sum_{i=1}^{n}\frac{Y_i\eta_i^2}{\left(\sum_{i=1}^{n}Y_i\eta_i^2\right)}\cdot\frac{1}{1+\frac{\tau}{\tau_{D_i}}}\cdot\frac{1}{\sqrt{1+\left(\frac{\omega_0}{z_0}\right)^2\cdot\frac{\tau}{\tau_{D_i}}}}. \tag{29}$$

Y_i is a molar fraction of i^{th} species. This formula becomes difficult to fit for more than two species as it is overparameterized. Thus it is preferable, if besides the diffusion properties, the species differ also in the photophysical properties. It might be either the emission wavelength (two-color FCS)[68] or the lifetime (time-resolved FCS).[69, 70]

3.2 FCS in the block copolymer micelles investigation

3.2.1 Molecular mass determination

As long as the static light scattering provides information on the mass-weighted molecular mass of the micelles (read-out parameter from the Zimm-plot), which is strongly influenced by the presence of tiny amount of high-molecular-mass aggregates, the use of FCS yields number-weighted characteristics. An independent estimation of both mass- and number-weighted molecular masses gives additional information on the polydispersity of the studied system.

The original principle of the molecular mass determination is quite simple. It is based on the titration of the micelles with the dye solution. Provided the distribution of

labels on the micelles is the Poisson type, the probability that a particular micelle is labeled by one or more dye molecules follows the equation:

$$P = 1 - e^{-\xi}, \tag{30}$$

where ξ is the dye-to-micelle ratio. Consequently, the number of observed particles depends on ξ as follows:

$$N = N_z (1 - e^{-\xi}), \tag{31}$$

where N_z is the particle number that would be observed if all micelles were labeled. Thus, the dependence of the particle number on the dye concentration is supposed to reveal clearly the point when ξ equals one (see Fig. 6), i.e. the dye concentration which corresponds to the concentration of the micelles c_m. As the concentration of the polymer c_p (the polymer samples were close to monodispersity) is known, the molecular mass of micelles can be easily calculated:

$$M_m = \frac{c_p}{c_m} \cdot M_p. \tag{32}$$

The molecular mass of micelles, provided the polymer is rather monodisperse, is a number weighted average.

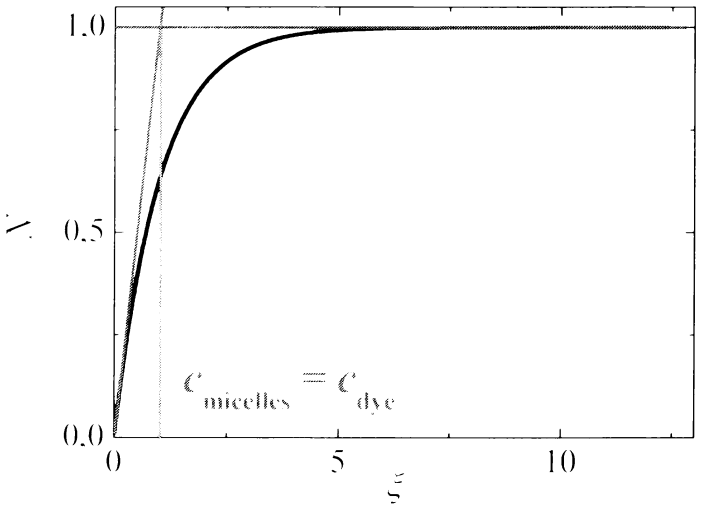

Figure 6. The theoretical dependence of the particle number on the dye-to-micelle ratio ξ. The green line shows the point where the concentration of the dye and the concentration of the micelles are equal.

Even though the idea is straightforward, it turned out that few additional factors need to be considered in order to obtain reliable data.

- Firstly, it is necessary to use the dye which binds strongly to micelles, i.e., the dye with high partition coefficient between the organic and water phase, so that the free dye would not contribute to the overall fluorescence signal and consequently would not cause any unwanted increase in the particle number. If there is any contribution from the solution, two particles have to be taken into account. If they, moreover, differ in their quantum yields, the problem complicates even more, as the quantum yields have to be measured independently.

  In our study, octadecylrhodamine B (ORB) was used as a fluorescent label. The detailed study[56, 57] reveals the partition coefficient in the range of 10^5, which allows to assume there is no additional signal from the solution. Furthermore, it was shown that when the dye-to-micelle ratio ξ becomes too high (i.e. several tens), the dye starts to be selfquenched by the presence of non-fluorescing H-dimers and by energy transfer from the monomers or J-dimers to the H-dimers, which causes again changes in quantum yield and finally (at ξ of several hundreds), the micelles become invisible for FCS. Since the solubility of ORB in water is very low, the water dispersed ORB chains form dimmers at very low concentration and the contribution from the fluorophores is self-quenched.
- Secondly, the quenching of the dye by micelles can cause deviations from the expected dependence on the dye-to-micelle ratio. This feature can be considered as if FCS "saw" only those particles that are labeled by two or more (three or more) dye molecules. Provided that twice labeled particles are observed, the dependence of the observed particles on ξ changes in the following manner:

$$N = N_A \left(1 - e^{-\xi} - \xi e^{-\xi}\right). \tag{33}$$

Fig. 7 illustrates the fact in detail. In this case, the concentration of the micelles can be calculated from N_A:

$$c_m = \frac{N_A}{N_A V}. \tag{34}$$

N_A is the Avogadro number and V is the size of the focus volume that has to be calibrated.

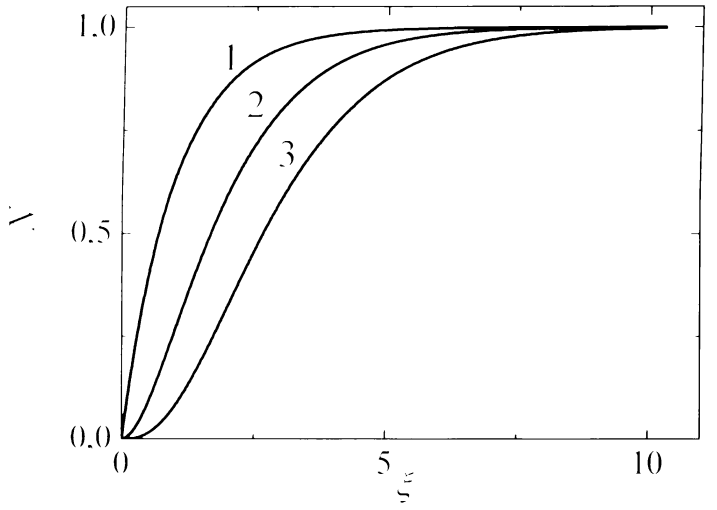

Figure 7. The theoretical dependences of particle number versus dye-to-micelle ratio ξ. Curve 1, 2 and 3 considers that one, two and three or more labelles, respectively, are needed so that FCS would "see" the micelles.

In the case of triblock copolymer micelles formed by the polystyrene core, poly(2-vinylpyridine) inner shell and polyoxyethylene outer shell, two different shapes of particle number-versus-ξ dependence were observed. In the acidic media, the shape corresponded well to the equation (31). In the alkaline media, however, the shape of the dependence reveals quenching of ORB by the deprotonated poly(2-vinylpyridine) and thus has to be fitted with the equation (33). (See Fig. 8.)[59] The very similar phenomena was observed also for polystyrene-*block*-poly(methacrylic acid) (PS-PMA) micelles.[56]

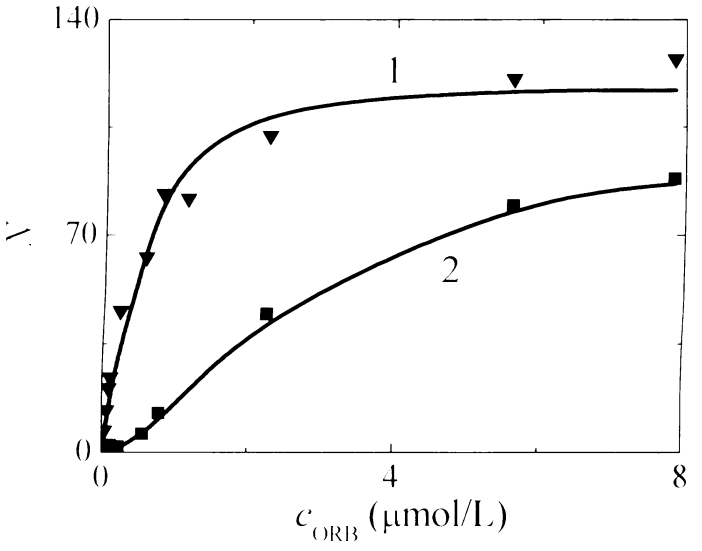

Figure 8. The dependence of the particle number on the ORB concentration. Curve 1 and 2 shows results obtained for polystyrene-*block*-poly(2-vinylpyridine)-polyoxyethylene micelles in acidic (pH=**2**) and basic (pH=**12**) media, respectively.

- Thirdly, the binding kinetics of the label has to be checked in order to be sure that the system is in equilibrium.

  In the case of binding kinetics of ORB to the PS-PMA micelles, it has been shown[57] that the whole process occurs in the range of several hours.
- Fourthly, since the dye is not localized in the center of gravity, but on the micellar surface, it has to be considered that not only the translational motion, but also the rotational motion causes fluctuations that may increase the number of observed particles. This phenomenon is under investigation.

3.2.2 Hydrodynamic radii determination

Apart from the number-averaged molecular mass, FCS also provides information on the hydrodynamic radius R_H of fluorescent species. The radius can be calculated from the diffusion coefficient using the formula:

$$R_H = \frac{kT}{6\pi\eta D}, \tag{35}$$

k is the Boltzman constant, T is temperature, η is solvent viscosity. However, the accuracy of the R_H evaluation is significantly lower from that based on QELS and small changes cannot be reliably monitored. The resolution in diffusion time is relatively poor. It has been shown that it has to be changed by factor 2 so that the change would be observable.

To demonstrate the R_H measurement, the PS-PMA micelles were studied under different conditions. As PS-PMA contain a weak polyelectrolyte block, the hydrodynamic radius depends on pH and ionic strength.[4, 71] In buffers with constant ionic strength, the observed pH-dependence (see Fig. 9) was in an agreement with the studies of analogous micellar systems studied by QELS.[4] Even though the increase in R_H is obvious, it has to be kept in mind that the changes are at the resolution edge.

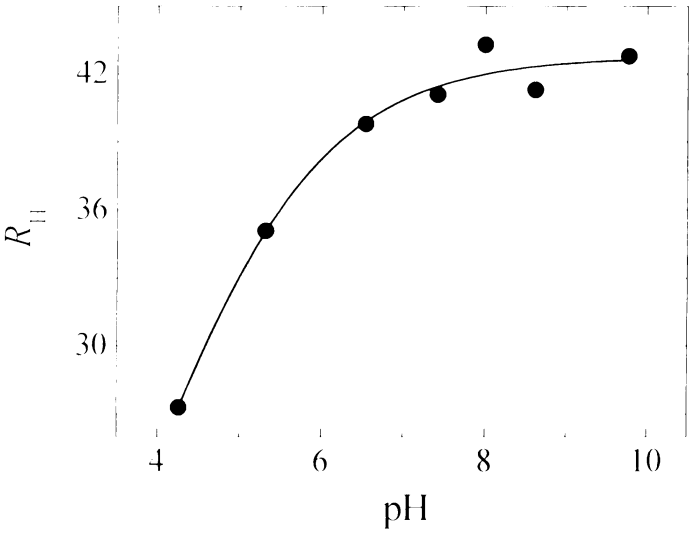

Figure 9. pH-dependent changes in the hydrodynamic radius of the PS-PMA micelles.

3.2.3 FCS versus QELS

Both FCS and QELS were used in polymer micelles studies.[18, 49, 56, 58-60] The results of the measurements suggest following comparison of the methods:

- QELS is applicable to all scattering species that differ in refractive index from the solution, while FCS can be used for those particles only that are fluorescently labeled. This fact makes, however, the FCS technique more

selective. It allows for studying labeled particles in the excess of other strongly scattering particles.

- The concentration needed for the QELS experiments is higher ($g.L^{-1}$) than for FCS which is in the nanomolar range. Moreover, the volume needed for FCS is quite small (tens microliters), thus the sample consumption is negligible.
- The stronger the scatterer is, the more it contributes to the overall signal. Since the scattering intensity strongly depends on the size, the fraction of particles with particular relaxation time is always intensity weighted. In the case of FCS, the signal is proportional to the number of fluorescent labels.
- The QELS autocorrelation function can be converted to the relaxation times or relaxation rates distribution by inverse Laplace transformation, whereas for FCS, the autocorrelation function has to be fitted by a mathematical model that assumes *a priori* what happens in the system.
- FCS, in contrast to QELS, is not designed to study systems with high polydispersity.
- FCS is a non-invasive technique and thus can be used also in vivo to reveal diffusion properties in living systems, which is going to be shown in the last part of this thesis.

Chapter IV

Fluorescence Correlation Spectroscopy in Two Dimensions: Application in Cellular Membrane Research

The fourth chapter deals with two-dimensional applications of FCS, i.e., diffusion in the membranes. Benda et al.[72] *elaborated a protocol called "z-scan" that enables to determine the lateral diffusion coefficient with a high precision compared to the standard FCS approach and does not require any external calibration.*

The approach proposed by Benda was used for supported phospholipids bilayers (SPBs). The method was first time also applied on the membranes of OLN-93 oligodendroglial cells in order to minimize experimental errors. An unexpected motion of the cellular membrane and other processes in living systems were studied under controllable conditions for the first time.

It was recently shown[73] *that a "single-waist" FCS experiment (i.e., an experiment performed with one size of the laser beam) is not appropriate for cells as the diffusion on the length scale of the beam radius can no more be considered free. This is due to the membrane organization that is beyond the microscope resolution and causes significant changes of the width of the ACF curves. It turned out that the z-scan method can be further utilized, so that it would provide additional information on membrane heterogeneities that a fluorescent membrane constituent interacts with.*

All these experiments were done in collaboration with the research team of prof. Yves Engelborghs (KU Leuven, Belgium) that contributed especially in the field of cell culturing and confocal imaging. The very first attempts to measure diffusion in the plasmatic membrane are summarized in the publication of Gielen et. al[74] *and the detailed utilization of the z-scan method can be found in the enclosed publication.*[75]

4.1 FCS data in two dimensions

In contrast to the three dimensional systems, the measurements of the lateral diffusion has to deal with a problem of proper positioning of the plane of interest in the

focal volume. As it is shown in the Schematics IV, the focused laser beam seems like if it had a kind of waist and therefore the number of observed particles and their diffusion time strongly depends on the relative z-position of the plane in the focus. It has been shown by Benda et al[72] that this can be overcome by the so called "z-scan" method which is based on moving the plane through the illuminated volume.

Schematics IV. Provided the pinhole is widely open, the focused volume appears to be Gaussian along the x and y axis and Lorentzian along the z-axis. Consequently, the number of fluorescent molecules as well as their diffusion time depends on the positioning of the plane of interest within the laser beam.

If the pinhole is widely open, the light-collection efficiency function ceases to play a significant role and the excitation intensity distribution is the only non-dynamic property that influences the effective shape of the focal volume. The effective light distribution can be no more treated as a three dimensional Gaussian, but the Lorentzian profile along the z-axis has to be considered, i.e.:

$$W(\vec{r}) = \frac{I_{ex}(\vec{r})}{I_0} = \frac{1}{\omega^2(z)} \exp\left(-\frac{x^2 + y^2}{\omega^2(z)}\right), \tag{36}$$

where $\omega^2(z) = \omega_0^2\left(1 + \frac{\lambda_0^2 \Delta z^2}{\pi^2 n^2 \omega_0^4}\right)$, λ_0 is the excitation wavelength, n is the refractive index and Δz is the relative distance of the plane of interest from the focus of the laser beam.

According to the volume shape, the observed read-out parameters (particle number and diffusion time) follow the parabolic behavior with respect to the z-position of the plane:

$$N = \pi c \omega_0^2 \left(1 + \frac{\lambda_0^2 \Delta z^2}{\pi^2 n^2 \omega_0^4} \right)$$
$$\tau_D = \frac{\omega_0^2}{4D} \left(1 + \frac{\lambda_0^2 \Delta z^2}{\pi^2 n^2 \omega_0^4} \right) \qquad (37, 38)$$

By fitting these formulas, the lateral diffusion coefficient and the surface concentration c can be evaluated. Apart from that, ω_0 can be calculated. Thus, the z-scan method provides information on the volume width without the need of any external calibration. The approach of scanning in the z-direction allows for precise positioning of the plane in the focus volume and thus, the accuracy of the lateral diffusion coefficient estimation is considerably improved.

The z-scan method has been mainly used for measurement of the lateral diffusion of labeled lipid molecules or proteins in phosholipid bilayers, either artificial on a kind of support, or *in vivo* in living cells.

4.2 Motivation for the membrane research of living cells via FCS

Some time ago, it was believed that the cellular membrane of eukaryotic cells is a homogeneous phospholipid sea of freely diffusing lipids and proteins. However, it has been shown[76-78] that this is far from truth since there seems to be a lot of heterogeneities caused by variable degrees of lipid miscibility.[79] According to this approach, plasma membrane contains lot of complexes, lipid domains and meshwork-like structures.

The so called "rafts", the liquid ordered domains built mainly from cholesterol and saturated lipids, attract lot of interest as they are thought to be involved in lot of dynamic processes, such as protein and lipid sorting, signal transduction, cell adhesion or pathogen entry.[80-86] Rafts' sizes rang from several tens of nanometers to several micrometers. The sizes around one micrometer can be observed in the model systems of giant unilamellar vesicles (GUVs)[87] or supported phospholipid bilayers (SPBs).[88] In cells, where they are mostly beyond the microscopic resolution, their presence was mainly observed indirectly. The evidence for their presence in the cellular membrane

comes from biochemical studies which show that some of the membrane constituents are insoluble in non-ionic detergents at low temperature. These so called detergent resistant membranes (DRMs) are known to be enriched with cholesterol and sphingolipids. It has been already indicated, however, that the solubility strongly depends on the used extraction conditions.[89-91] As this method requires the total destruction of cells and studies lipid solubility at temperature far from physiological conditions, the need of non-invasive approach being able to work *in vivo* is crucial. Consequently, the diffusion of lipids and proteins can no more be considered free like in the case of the lipid sea because the partitioning between different lipid phases and different diffusion rates in the individual phases have to be taken into account.

Apart from rafts, meshwork structures, such as membrane-associated actin cytoskeleton (forming fences) can have a considerable influence on the diffusion because it causes a confinement of the transmembrane proteins anchored in the actin skeleton.[92]

All the cellular experiments were held in oligodendrocytes (OLGs), which are the myelin producing cells of central nervous system. They extend a complex array of processes projecting outward the cell body. They form segments of highly specialized membranes that enwraps axons, i.e., the myelin sheath, which is essential for the fast saltatory conduction of action potentials along the nerve cells and thus for proper functioning of the nervous system. Abnormalities in myelin development, disturbance or destruction of its structure lead to the severe neurological symptoms observed in diseases such as multiple sclerosis.[93-95] In OLGs, the formation of lipid rafts has been postulated to be a mechanism of membrane subdomain organization, important for compartmentalization of signaling molecules as well as for sorting of myelin components. Presently, however, information on rafts in OLGs is based on detergent extraction only, which is justifiably doubted to give reliable information on molecular organization of the multicomponent cell surface.[96-101]

The FCS approach together with confocal scanning microscopy appears to be a promising non-invasive tool in cellular membrane research. It is commonly applied in the artificial and native cellular membranes to study raft properties[102]and eventually, first attempts reveal its capabilities in the membrane heterogeneity examination.[74]

4.3 FCS diffusion law

The standard FCS experiment is normally carried out with a single size of the laser beam. This approach is sufficient in the case of free diffusion. If the diffusion is hindered, however, it turns out that on the length scale bigger than the size of possible obstacles, the free diffusion law, i.e., $\tau_D = \frac{\omega^2}{4D}$, is no more observed. Consequently, as the diffusion time is not directly proportional to the size of the illuminated area, the proper information on diffusion behavior can be obtained if a variable beam size is used (multi-waist approach). This is necessary for the study of cellular membrane since the obstacles (domains, fences) are usually smaller than the laser radius.

Wawrezinieck et al.[73] showed in the multi-waist experiments and mainly by simulations how the presence of domains or meshwork influences the dependence of the observed diffusion time (FWHM of the ACF). It has been revealed that in the case of the domains or the fences beyond the resolution of diffraction limited confocal microscopy, the shape of ACFs remains practically unchanged compared to the free lateral diffusion. The only observable parameter that undergoes changes is the fullwidth in half maximum, i.e., the apparent diffusion time. Plotting the diffusion time against the surface of illuminated area provides then information on the so called "FCS diffusion law". It has been shown that different heterogeneities change the plot in different ways.

As already mentioned, two phenomenological models were studied by simulations (see Schematics V):

- Domains (rafts) in which the flourophore (protein, lipid or lipid-like molecule) is partitioned, i.e., the fluorophore diffuses freely but with different rates in the raft and non-raft regions. Apart from that, different degrees of confinement in rafts were simulated, i.e., the raft/non-raft interface differs in the degree of permeability.
- Meshwork that consists of compartments separated by energy barriers (fences). The flourophore diffuses freely in the compartments, but an additional energy is needed to cross the barrier, i.e., the probability of the crossing is lowered.

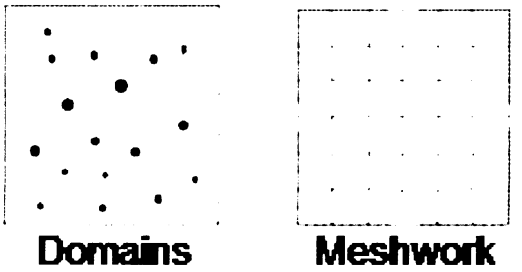

Schematics V. Schematic picture of two phenomenological models: Domains: submicrometer phases with different diffusion properties (black circles). Meshwork: Fences compartmentalizing the membrane (black lines). Yellow circle represents the size of the laser beam.

Both the simulations and the experiments suggest that the "FCS diffusion law" can be generally written as:[73]

$$\tau_D^{app} = t_0 + \frac{1}{4D_{eff}}\omega^2, \tag{39}$$

τ_D^{app} is the apparent diffusion time – full width in the half maximum of the ACF, it approaches the real diffusion time in the case of free diffusion. t_0 and D_{eff} are constants related to phenomenological models of the processes occuring in the membrane. $t_0 > 0$, in the case of microdomains and $t_0 < 0$, in the case of meshwork.

4.4 Application of the z-scan method

According to the above mentioned facts, it can be concluded that in the case of cellular membranes the single-waist experiment is principally not sufficient to reveal what happens on the nanometer length scale. To be able to extract information on the diffusion in the heterogeneous systems like cellular membranes are, the waist size needs to be changed. This requires either a beam expander or underfilling of the objective, which may be a technical problem for most commercial microscopes.

The z-scan method, besides the precise positioning of the membrane in the laser beam, can be used to approach the "FCS diffusion law" without any technical inconvenience. When the membrane is moved out from the waist of the laser focus the illuminated area increases. Consequently, the diffusion time can be obtained as a function of the illuminated spot size.

Apart from the fact that the z-scan approach allows for the illuminated area expansion, it also provides information on its size. This is based on the assumption that the size is directly proportional to the number of observed particles: $\omega^2 = \frac{N}{N_0}\omega_0^2$, where N_0 is the number of particles in the waist of the laser beam and ω_0 is the radius of the laser beam waist. Consequently, the equation (39) can be rewritten:

$$\tau_D^{app} = t_0 + \frac{\omega_0^2}{4D_{cell}} \cdot \frac{N}{N_0}. \qquad (40)$$

For the experiments in the bottom membrane of the OLN-93 oligodendroglial cells, the putative "non-raft" marker DiD (1,1'-dioctadecyl-3,3,3',3'-tetramethylindodicarbocyanine perchlorate) was chosen. The read-out parameters of the z-scan experiment follows well the theoretical relations (Fig. 10).

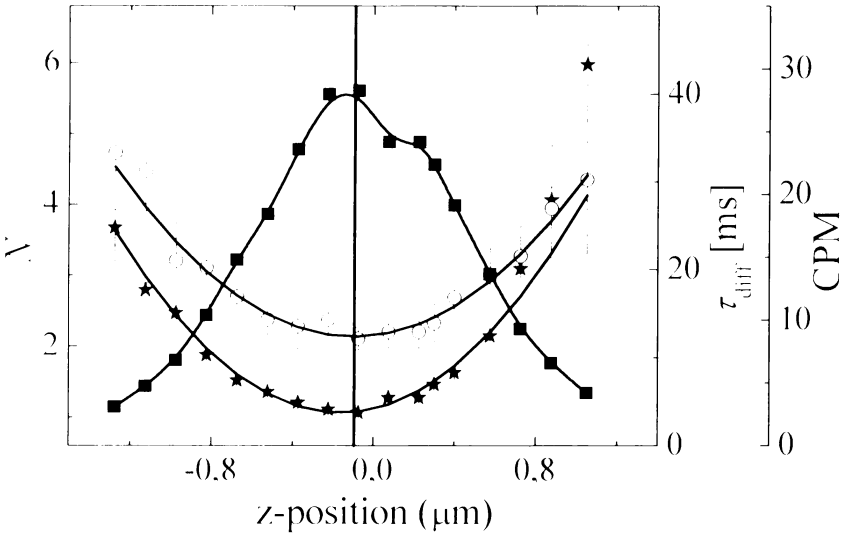

Figure 10. Z-scan for DiD in the bottom membrane of OLN-93 oligodendroglial cells. CPM: counts per second per molecule: ■: CPM; : τ_D; ★: N. Error bars represent standard errors.

The plots of the apparent diffusion time versus the relative particle number N/N_0 reveal a positive intercept in the range of few milliseconds (see Fig. 11). In order to have an idea how significant the result is, the same experiment was performed on the artificial membrane, supported phospholipid bilayer (SPB) (consisting of

dioleoylphosphatidylcholin and dioleoylphosphatidylserin in the molar ratio 4:1) labeled with the same fluorophore. As a support, mica was used, which is known to be flat on the atomic level. Fig. 11 shows the clear difference in the intercepts that in the case of the artificial membrane, where the diffusion is expected to be free, does not exceed 1 ms (see Table I).

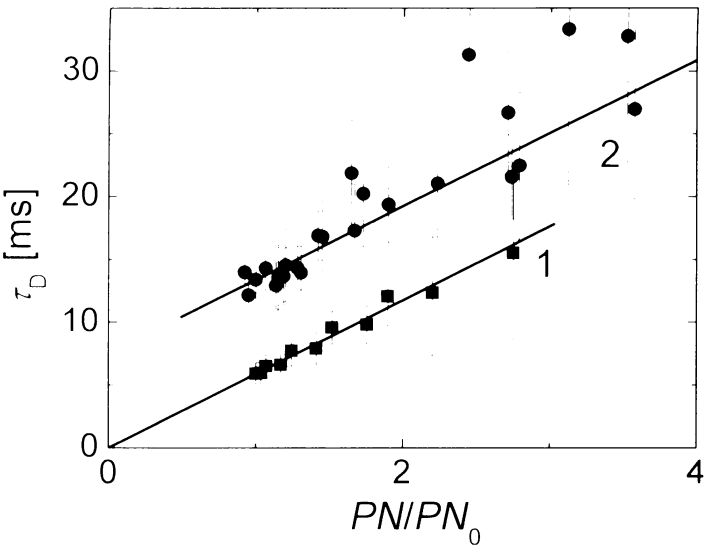

Figure 11. Plots of the diffusion time versus the relative particle number obtained for DiD in DOPC:DOPS SPBs on mica (■) and in OLN-93 (●). Error bars represent standard errors.

System	t_0 [ms]	Δt_0 [ms]	D_{eff} [$\mu m^2.s^{-1}$]	ΔD_{eff} [$\mu m^2.s^{-1}$]
SPB on mica	0,8	0,5	5,4	1,1
SPB on mica	0	fixed	4,8	0,4
Cells	5,4	0,5	4,4	1,1

Table I. Effective diffusion coefficients of DiD in SPBs and in OLN-93 oligodendroglial cells obtained from the *z*-scan at room temperature. Errors are reported as confidence intervals (at 0,95 confidence level).

Apparently, the intercepts obtained for the cells are considerably higher than those obtained for SPBs on mica. This result supports the idea of rafts presence in the cellular membrane. According to the simulations and provided that the idea of domains

(rafts) smaller than the illuminated area is valid, the intercept can be expressed as follows:

$$t_0 \approx 2 \cdot \alpha \cdot \left(\tau_{\text{conf}} - \tau_D^{\text{domain}}\right), \tag{41}$$

α is the partition coefficient of the dye between raft and non-raft regions, τ_{conf} is the confinement time, the average time that a molecule placed in the centre of the circular domain needs to escape from it, τ_D^{domain} is the diffusion time in the domain, usually much smaller than the confinement time. This suggests that DiD expected to be preferentially a non-raft marker is partitioned in the both phases and that the domains are not totally permeable for the dye.

The effective diffusion coefficient is related to the partition coefficient and the "free diffusion coefficient" D_{free}:

$$D_{\text{eff}} = (1 - \alpha) D_{\text{free}}. \tag{42}$$

In the case of high α, i.e., the probe is concentrated in rafts, D_{free} equals to the diffusion coefficient in the non-raft region, in the opposite case, D_{free} is lowered by factor that takes the size and density of impermeable domains into account.

Finally, since it is believed that the presence of cholesterol is crucial for rafts formation, the cellular cholesterol was depleted by treating the cells with β-cyklodextrin. The values of effective diffusion coefficients and intercepts show only a slight increase of intercept in the case of depleted cells, whereas the effective diffusion coefficient remains constant within the experimental error.

Provided that the partition coefficient does not change upon depletion, which is supported by the fact that the effective diffusion coefficient remains almost unchanged, the results can be explained in the following way:

i) The diffusion of DiD in the non-raft areas is not affected since the effective diffusion coefficient is not changed.

ii) An increase in t_0 suggests either increasing confinement time, which would correspond to the rafts' growth, or a decrease in the diffusion time in the domains. If the later is the case, then the results show that the diffusion in the liquid ordered domains is accelerated, which is in agreement with generally observable phenomena.[102] This effect is, however, the less observable the less the dye is present in rafts.

Conclusions

The thesis introduced two techniques, solvent relaxation that rises from the very basic understanding of photophysics and the fluorescence correlation spectroscopy that at the first sight uses the phenomena of fluorescence in order to merely visualize the studied system. Both the methods, however, give information on molecular dynamics. The relaxation "sees" kinetics of the solvent rearrangement, whereas FCS visualizes the diffusion.

Relaxation of the solvent seems to be a very useful tool in polymer science since it turns out to be sensitive to the presence of water molecules and their mobility in the micellar shell. The changes in microorganization of the shell, i.e., in water content and in hydration of polymer chains, are hardly accessible by other methods.

FCS is a complementary technique to the scattering methods, however, light scattering approach is already well established, whereas FCS results depend tremendously on the photophysics of the chosen dye and also on its location. The major advantage is that FCS is not much affected by big, strongly scattering particles (for instance aggregates) and that gives number-weighted averages of molecular mass and hydrodynamic radii. FCS, furthermore, works in lower concentration range and even if the refractive index increment is insufficient for scattering techniques. From the opposite point of view, polymer micelles are simple model systems that can be well used for testing of the method.

Whereas FCS measurements of micellar systems in three dimensions (i.e. in the solution) do not bring any unexpected breakthrough compared to the standard techniques, the method being applied in two-dimensions, i.e. in the membranes, moreover, in the living systems, cannot be replaced by any other method.

The utilization of FCS for the exploration of membranes in living cells, which is discussed in the last chapter, is doubtlessly a unique approach to learn about membrane microheterogeneities that are beyond the resolution of confocal microscopy.

References

1. Stepanek, M.; Podhajecka, K.; Tesarova, E.; Prochazka, K.; Tuzar, Z.; Brown, W., Hybrid polymeric micelles with hydrophobic cores and mixed polyelectrolyte/nonelectrolyte shells in aqueous media. 1. Preparation and basic characterization. *Langmuir* **2001,** 17, (14), 4240-4244.

2. Podhajecka, K.; Stepanek, M.; Prochazka, K.; Brown, W., Hybrid polymeric micelles with hydrophobic cores and mixed polyelectrolyte/nonelectrolyte shells in aqueous media. 2. Studies of the shell behavior. *Langmuir* **2001,** 17, (14), 4245-4250.

3. Tsitsilianis, C.; Voulgaris, D.; Stepanek, M.; Podhajecka, K.; Prochazka, K.; Tuzar, Z.; Brown, W., Polystyrene/poly(2-vinylpyridine) heteroarm star copolymer micelles in aqueous media and onion type micelles stabilized by diblock copolymers. *Langmuir* **2000,** 16, (17), 6868-6876.

4. Stepanek, M.; Prochazka, K.; Brown, W., Time-dependent behavior of block polyelectrolyte micelles in aqueous media studied by potentiometric titrations, QELS and fluorometry. *Langmuir* **2000,** 16, (6), 2502-2507.

5. Stepanek, M.; Podhajecka, K.; Prochazka, K.; Teng, Y.; Webber, S. E., Fluorometric and ultraviolet-visible absorption study of poly(methacrylic acid) shells of high-molar-mass block copolymer micelles. *Langmuir* **1999,** 15, (12), 4185-4193.

6. Tuzar, Z.; Kratochvil, P., *Advances in colloid and interface science* **1976,** 6, 201.

7. Tuzar, Z.; Kratochvil, P., In *Surface and Colloid Science*, Matijevic, E., Ed. Plenum Press: New York, 1993; Vol. 15, p 1.

8. Riess, G.; Heuretz, G.; Bahadur, P., In *Encyclopedia of Polymer Science and Engineering*, 2 ed.; Mark, H.; Bikales, N., M.; Overberger, C., G.; Menges, G., Eds. Wiley: New York, 1985; Vol. 2, p 324.

9. Price, C., In *Developments in Block Copolymers*, Goodman, I., Ed. Applied Science Publishers: London - New York, 1989; Vol. 1, p 39.

10. Tian, M. M.; Qin, A. W.; Ramireddy, C.; Webber, S. E.; Munk, P.; Tuzar, Z.; Prochazka, K., Hybridization of Block-Copolymer Micelles. *Langmuir* **1993,** 9, (7), 1741-1748.

11. Kiserow, D.; Prochazka, K.; Ramireddy, C.; Tuzar, Z.; Munk, P.; Webber, S. E., Fluorometric and Quasi-Elastic Light-Scattering Study of the Solubilization of

Nonpolar Low-Molar Mass Compounds into Water-Soluble Block-Copolymer Micelles. *Macromolecules* **1992,** 25, (1), 461-469.

12. Zhang, L. F.; Eisenberg, A., Thermodynamic vs kinetic aspects in the formation and morphological transitions of crew-cut aggregates produced by self-assembly of polystyrene-b-poly(acrylic acid) block copolymers in dilute solution. *Macromolecules* **1999,** 32, (7), 2239-2249.

13. Zhang, L. F.; Eisenberg, A., Formation of crew-cut aggregates of various morphologies from amphiphilic block copolymers in solution. *Polymers for Advanced Technologies* **1998,** 9, (10-11), 677-699.

14. Luo, L. B.; Eisenberg, A., Thermodynamic stabilization mechanism of block copolymer vesicles. *Journal of the American Chemical Society* **2001,** 123, (5), 1012-1013.

15. Shen, H. W.; Eisenberg, A., Morphological phase diagram for a ternary system of block copolymer PS310-b-PAA(52)/dioxane/H2O. *Journal of Physical Chemistry B* **1999,** 103, (44), 9473-9487.

16. Teng, Y.; Morrison, M. E.; Munk, P.; Webber, S. E.; Prochazka, K., Release kinetics studies of aromatic molecules into water from block polymer micelles. *Macromolecules* **1998,** 31, (11), 3578-3587.

17. Stepanek, M.; Krijtova, K.; Prochazka, K.; Teng, Y.; Webber, S. E.; Munk, P., Solubilization and release of hydrophobic compounds from block copolymer micelles. I. Partitioning of pyrene between polyelectrolyte micelles and the aqueous phase. *Acta Polymerica* **1998,** 49, (2-3), 96-102.

18. Matejicek, P.; Podhajecka, K.; Humpolickova, J.; Uhlik, F.; Jelinek, K.; Limpouchova, Z.; Prochazka, K.; Spirkova, M., Polyelectrolyte behavior of polystyrene-block-poly(methacrylic acid) micelles in aqueous solutions at low ionic strength. *Macromolecules* **2004,** 37, (26), 10141-10154.

19. Sheiko, S. S., Imaging of polymers using scanning force microscopy: From superstructures to individual molecules. *New Developments in Polymer Analytics Ii* **2000,** 151, 61-174.

20. Sheiko, S. S.; Moller, M., Visualization of macromolecules - A first step to manipulation and controlled response. *Chemical Reviews* **2001,** 101, (12), 4099-4123.

21. Binnig, G.; Quate, C. F.; Gerber, C., Atomic Force Microscope. *Physical Review Letters* **1986,** 56, (9), 930-933.

22. Hartley, P. G.; Scales, P. J., Electrostatic properties of polyelectrolyte modified surfaces studied by direct force measurement. *Langmuir* **1998,** 14, (24), 6948-6955.

23. Zhmud, B. V.; Meurk, A.; Bergstrom, L., Evaluation of surface ionization parameters from AFM data. *Journal of Colloid and Interface Science* **1998,** 207, (2), 332-343.

24. Briscoe, W. H.; Horn, R. G., Direct measurement of surface forces due to charging of solids immersed in a nonpolar liquid. *Langmuir* **2002,** 18, (10), 3945-3956.

25. Sykora, J.; Mudogo, V.; Hutterer, R.; Nepras, M.; Vanerka, J.; Kapusta, P.; Fidler, V.; Hof, M., ABA-C-15: A new dye for probing solvent relaxation in phospholipid bilayers. *Langmuir* **2002,** 18, (24), 9276-9282.

26. Hutterer, R.; Hof, M., Probing ethanol-induced phospholipid phase transitions by the polarity sensitive fluorescence probes Prodan and Patman. *Zeitschrift Fur Physikalische Chemie-International Journal of Research in Physical Chemistry & Chemical Physics* **2002,** 216, 333-346.

27. Hutterer, R.; Hof, M., Dynamics in diether lipid bilayers and interdigitated bilayer structures studied by time-resolved emission spectra, decay time and anisotropy profiles. *Journal of Fluorescence* **2001,** 11, (3), 227-236.

28. Hutterer, R.; Kramer, K.; Schneider, F. W.; Hof, M., The localization of the local anesthetic tetracaine in phospholipid vesicles: A fluorescence quenching and resonance energy transfer study. *Chemistry and Physics of Lipids* **1997,** 90, (1-2), 11-23.

29. Hutterer, R.; Parusel, A. B. J.; Hof, M., Solvent relaxation of Prodan and Patman: A useful tool for the determination of polarity and rigidity changes in membranes. *Journal of Fluorescence* **1998,** 8, (4), 389-393.

30. Hutterer, R.; Schneider, F. W.; Hermens, W. T.; Wagenvoord, R.; Hof, M., Binding of prothrombin and its fragment 1 to phospholipid membranes studied by the solvent relaxation technique. *Biochimica Et Biophysica Acta-Biomembranes* **1998,** 1414, (1-2), 155-164.

31. Hutterer, R.; Schneider, F. W.; Hof, M., Anisotropy and lifetime profiles for n-anthroyloxy fatty acids: A fluorescence method for the detection of bilayer interdigitation. *Chemistry and Physics of Lipids* **1997,** 86, (1), 51-64.

32. Hutterer, R.; Schneider, F. W.; Lanig, H.; Hof, M., Solvent relaxation behaviour of n-anthroyloxy fatty acids in PC-vesicles and paraffin oil: A time-resolved emission spectra study. *Biochimica Et Biophysica Acta-Biomembranes* **1997,** 1323, (2), 195-207.

33. Hutterer, R.; Schneider, F. W.; Sprinz, H.; Hof, M., Binding and relaxation behaviour of Prodan and Patman in phospholipid vesicles: A fluorescence and H-1 NMR study. *Biophysical Chemistry* **1996,** 61, (2-3), 151-160.

34. Hof, M., In *Solvent Relaxation in Biomembranes (Applied Fluorescence in Chemistry, Biology and Medicine)*, Rettig, W., Ed. Springer-Verlag: Berlin, 1999; p 439.

35. Hof, M.; Hutterer, R., Solvent relaxation of fluorescent labels as a new tool for the detection of polarity and rigidity changes in membranes. *Czechoslovak Journal of Physics* **1998,** 48, (4), 435-441.

36. Hof, M.; Hutterer, R.; Perez, N.; Ruf, H.; Schneider, F. W., Influence of Vesicle Curvature on Fluorescence Relaxation Kinetics of Fluorophores. *Biophysical Chemistry* **1994,** 52, (2), 165-172.

37. Bieze, T. W. N.; Barnes, A. C.; Huige, C. J. M.; Enderby, J. E.; Leyte, J. C., Distribution of Water around Poly(Ethylene Oxide) - a Neutron-Diffraction Study. *Journal of Physical Chemistry* **1994,** 98, (26), 6568-6576.

38. Humpolickova, J.; Stepanek, M.; Prochazka, K.; Hof, M., Solvent relaxation study of pH-dependent hydration of poly(oxyethylene) shells in polystyrene-block-poly(2-vinylpyridine)-block-poly(oxyethylene) micelles in aqueous solutions. *Journal of Physical Chemistry A* **2005,** 109, (48), 10803-10812.

39. Arzhantsev, S.; Ito, N.; Heitz, M.; Maroncelli, M., Solvation dynamics of coumarin 153 in several classes of ionic liquids: cation dependence of the ultrafast component. *Chemical Physics Letters* **2003,** 381, (3-4), 278-286.

40. Ingram, J. A.; Moog, R. S.; Ito, N.; Biswas, R.; Maroncelli, M., Solute rotation and solvation dynamics in a room-temperature ionic liquid. *Journal of Physical Chemistry B* **2003,** 107, (24), 5926-5932.

41. Ito, N.; Arzhantsev, S.; Heitz, M.; Maroncelli, M., Solvation dynamics and rotation of coumarin 153 in alkylphosphonium ionic liquids. *Journal of Physical Chemistry B* **2004,** 108, (18), 5771-5777.

42. Fee, R. S.; Maroncelli, M., Estimating the Time-Zero Spectrum in Time-Resolved Emission Measurements of Solvation Dynamics. *Chemical Physics* **1994,** 183, (2-3), 235-247.

43. Yang, M.; Richert, R., Observation of heterogeneity in the nanosecond dynamics of a liquid. *Journal of Chemical Physics* **2001,** 115, (6), 2676-2680.

44. Richert, R., Spectral diffusion in liquids with fluctuating solvent responses: Dynamical heterogeneity and rate exchange. *Journal of Chemical Physics* **2001,** 115, (3), 1429-1434.

45. Demas, J., N., *Excited states lifetime measurements*. 1 ed.; Academic press: New York, 1983.

46. Lakowicz, J. R., *Principles of Fluorescence Spectroscopy*. 2 ed.; Kluwer Academic: New York, 1999.

47. Valeur, B., *Molecular Fluorescence - Principles and Applications*. 1 ed.; Wiley-VCH Verlag: New York, 2001.

48. Martin, T. J.; Prochazka, K.; Munk, P.; Webber, S. E., pH-dependent micellization of poly(2-vinylpyridine)-block-poly(ethylene oxide). *Macromolecules* **1996,** 29, (18), 6071-6073.

49. Stepanek, M.; Matejicek, P.; Humpolickova, J.; Prochazka, K., Reversible aggregation of polystyrene-block-poly(2-vinylpyridine)-block-poly(ethylene oxide) block copolymer micelles in acidic aqueous solutions. *Langmuir* **2005,** 21, (23), 10783-10790.

50. Kral, T.; Widerak, K.; Langner, M.; Hof, M., Propidium iodide and PicoGreen as dyes for the DNA fluorescence correlation spectroscopy measurements. *Journal of Fluorescence* **2005,** 15, (2), 179-183.

51. Kral, T.; Hof, M.; Jurkiewicz, P.; Langner, M., Fluorescence correlation spectroscopy (FCS) as a tool to study DNA condensation with hexadecyltrimethylammonium bromide (HTAB). *Cellular & Molecular Biology Letters* **2002,** 7, (2), 203-211.

52. Kral, T.; Langner, M.; Benes, M.; Baczynska, D.; Ugorski, M.; Hof, M., The application of fluorescence correlation spectroscopy in detecting DNA condensation. *Biophysical Chemistry* **2002,** 95, (2), 135-144.

53. Kral, T.; Hof, M.; Langner, M., The effect of spermine on plasmid condensation and dye release observed by fluorescence correlation spectroscopy. *Biological Chemistry* **2002,** 383, (2), 331-335.

54. Bahns, J. T.; Liu, C. M.; Chen, L. H., Characterizing specific phage-protein interactions by fluorescence correlation spectroscopy. *Protein Science* **2004,** 13, (10), 2578-2587.

55. Lagerkvist, A. C.; Foldes-Papp, Z.; Persson, M. A. A.; Rigler, R., Fluorescence correlation spectroscopy as a method for assessment of interactions between phage displaying antibodies and soluble antigen. *Protein Science* **2001,** 10, (8), 1522-1528.

56. Humpolickova, J.; Prochazka, K.; Hof, M.; Tuzar, Z.; Spirkova, M., Fluorescence correlation spectroscopy using octadecylrhodamine B as a specific micelle-binding fluorescent tag: Light scattering and tapping mode atomic force microscopy studies of amphiphilic water-soluble block copolymer micelles. *Langmuir* **2003,** 19, (10), 4111-4119.

57. Humpolickova, J.; Prochazka, K.; Hof, M., Octadecylrhodamine B as a specific micelle-binding fluorescent tag for fluorescence correlation spectroscopy studies of amphiphilic water-soluble block copolymer micelles. Spectroscopic behavior in aqueous media. *Collection of Czechoslovak Chemical Communications* **2003,** 68, (11), 2105-2119.

58. Stepanek, M.; Matejicek, P.; Humpolickova, J.; Havrankova, J.; Podhajecka, K.; Spirkova, M.; Tuzar, Z.; Tsitsilianis, C.; Prochazka, K., New insights on the solution behavior and self-assembly of polystyrene/poly(2-vinylpyridine) 'hairy' heteroarm star copolymers with highly asymmetric arms in polar organic and aqueous media. *Polymer* **2005,** 46, (23), 10493-10505.

59. Stepanek, M.; Humpolickova, J.; Prochazka, K.; Hof, M.; Tuzar, Z.; Spirkova, M.; Wolff, T., Light scattering, atomic force microscopy and fluorescence correlation spectroscopy studies of polystyrene-block-poly(2-vinylpyridine)-block-poly(ethylene oxide) micelles. *Collection of Czechoslovak Chemical Communications* **2003,** 68, (11), 2120-2138.

60. Matejicek, P.; Humpolickova, J.; Prochazka, K.; Tuzar, Z.; Spirkova, M.; Hof, M.; Webber, S. E., Hybrid block copolymer micelles with partly hydrophobically modified polyelectrolyte shells in polar and aqueous media: Experimental study using fluorescence correlation spectroscopy, time-resolved fluorescence, light scattering, and atomic force microscopy. *Journal of Physical Chemistry B* **2003,** 107, (32), 8232-8240.

61. Magde, D.; Elson, E.; Webb, W. W., Thermodynamic fluctuations in a reacting system - measurement by fluorescence correlation spectroscopy. *Physical Review Letters* **1972,** 29, (11), 705-708.

62. Elson, E.; Magde, D., Fluorescence Correlation Spectroscopy. I.Conceptual Basis and Theory. *Biopolymers* **1974,** 13, 1-27.

63. Magde, D.; Elson, E., Fluorescence Correlation Spectroscopy. II.An Experimental Realization. *Biopolymers* **1974,** 13, 29-61.

64. Thompson, N. L., Fluorescence Correlation Spectroscopy. In *Topics in Fluorescence Spectroscopy*, Lakowicz, J. R., Ed. Plenum Press: New York, 1991; Vol. 1, pp 337-378.

65. Widengren, J.; Rigler, R., Review - Fluorescence correlation spectroscopy as a tool to investigate chemical reactions in solutions and on cell surfaces. *Cellular and Molecular Biology* **1998,** 44, (5), 857-879.

66. Widengren, J.; Mets, U.; Rigler, R., Fluorescence Correlation Spectroscopy of Triplet-States in Solution - a Theoretical and Experimental-Study. *Journal of Physical Chemistry* **1995,** 99, (36), 13368-13379.

67. Schwille, P., Fluorescence correlation spectroscopy and its potential for intracellular applications. *Cell Biochemistry and Biophysics* **2001,** 34, (3), 383-408.

68. Schwille, P.; MeyerAlmes, F. J.; Rigler, R., Dual-color fluorescence cross-correlation spectroscopy for multicomponent diffusional analysis in solution. *Biophysical Journal* **1997,** 72, (4), 1878-1886.

69. Bohmer, M.; Wahl, M.; Rahn, H. J.; Erdmann, R.; Enderlein, J., Time-resolved fluorescence correlation spectroscopy. *Chemical Physics Letters* **2002,** 353, (5-6), 439-445.

70. Benda, A.; Hof, M.; Wahl, M.; Patting, M.; Erdmann, R.; Kapusta, P., TCSPC upgrade of a confocal FCS microscope. *Review of Scientific Instruments* **2005,** 76, (3), -.

71. Karymov, M. A.; Prochazka, K.; Mendenhall, J. M.; Martin, T. J.; Munk, P.; Webber, S. E., Chemical attachment of polystyrene-block-poly(methacrylic acid) micelles on a silicon nitride surface. *Langmuir* **1996,** 12, (20), 4748-4753.

72. Benda, A.; Benes, M.; Marecek, V.; Lhotsky, A.; Hermens, W. T.; Hof, M., How to determine diffusion coefficients in planar phospholipid systems by confocal fluorescence correlation spectroscopy. *Langmuir* **2003,** 19, (10), 4120-4126.

73. Wawrezinieck, L.; Rigneault, H.; Marguet, D.; Lenne, P. F., Fluorescence correlation spectroscopy diffusion laws to probe the submicron cell membrane organization. *Biophysical Journal* **2005,** 89, (6), 4029-4042.

74. Gielen, E.; Vercammen, J.; Sykora, J.; Humpolickova, J.; vandeVen, M.; Benda, A.; Hellings, N.; Hof, M.; Engelborghs, Y.; Steels, P.; Ameloot, M., Diffusion of sphingomyelin and myelin oligodendrocyte glycoprotein in the membrane of OLN-93

oligodendroglial cells studied by fluorescence correlation spectroscopy. *Comptes Rendus Biologies* **2005,** 328, (12), 1057-1064.

75. Humpolickova, J.; Gielen, E.; Benda, A.; Fagulova, V.; Vercammen, J.; vandeVen, M.; Hof, M.; Ameloot, M.; Engelborghs, Y., Probing microheterogeneities within cellular membranes by Z-scanning fluorescence correlation spectroscopy. *Biophysical Journal* **2006,** accepted.

76. Lai, E. C., Lipid rafts make for slippery platforms. *Journal of Cell Biology* **2003,** 162, (3), 365-370.

77. Klausner, R. D.; Kleinfeld, A. M.; Hoover, R. L.; Karnovsky, M. J., Lipid Domains in Membranes - Evidence Derived from Structural Perturbations Induced by Free Fatty-Acids and Lifetime Heterogeneity Analysis. *Journal of Biological Chemistry* **1980,** 255, (4), 1286-1295.

78. Karnovsky, M. J.; Kleinfeld, A. M.; Hoover, R. L.; Klausner, R. D., The Concept of Lipid Domains in Membranes. *Journal of Cell Biology* **1982,** 94, (1), 1-6.

79. Kusumi, A.; Koyama-Honda, I.; Suzuki, K., Molecular dynamics and interactions for creation of stimulation-induced stabilized rafts from small unstable steady-state rafts. *Traffic* **2004,** 5, (4), 213-230.

80. Jahn, R.; Bock, A.; Breiner, K. M.; Breunig, K. D.; Bujard, H.; Campos-Ortega, J.; Ganten, D.; Grummt, I.; Gruss, P.; Goridis, C.; Huber, R.; Hoch, M.; Jackle, H.; Kahmann, R.; Koch-Brandt, C.; Leptin, M.; Michel, H.; Noegel, A.; Neher, E.; Nusslein-Volhard, C.; Pfanner, N.; Sandhoff, K.; Schoen, A.; Schwille, P.; Simons, K.; Zrenner, E., Distinguished scientists back Germany's DFG. *Nature* **2000,** 404, (6781), 922-922.

81. Simons, K.; Toomre, D., Lipid rafts and signal transduction. *Nature Reviews Molecular Cell Biology* **2000,** 1, (1), 31-39.

82. Maxfield, F. R., Plasma membrane microdomains. *Current Opinion in Cell Biology* **2002,** 14, (4), 483-487.

83. Edidin, M., The state of lipid rafts: From model membranes to cells. *Annual Review of Biophysics and Biomolecular Structure* **2003,** 32, 257-283.

84. Brown, D. A.; London, E., Functions of lipid rafts in biological membranes. *Annual Review of Cell and Developmental Biology* **1998,** 14, 111-136.

85. Brown, D. A.; London, E., Structure and function of sphingolipid- and cholesterol-rich membrane rafts. *Journal of Biological Chemistry* **2000,** 275, (23), 17221-17224.

86. Mukherjee, S.; Maxfield, F. R., Membrane domains. *Annual Review of Cell and Developmental Biology* **2004,** 20, 839-866.

87. Bagatolli, L. A.; Gratton, E., Two photon fluorescence microscopy of coexisting lipid domains in giant unilamellar vesicles of binary phospholipid mixtures. *Biophysical Journal* **2000,** 78, (1), 290-305.

88. Crane, J. M.; Tamm, L. K., Role of cholesterol in the formation and nature of lipid rafts in planar and spherical model membranes. *Biophysical Journal* **2004,** 86, (5), 2965-2979.

89. Banerjee, P.; Joo, J. B.; Buse, J. T.; Dawson, G., Differential Solubilization of Lipids Along with Membrane-Proteins by Different Classes of Detergents. *Chemistry and Physics of Lipids* **1995,** 77, (1), 65-78.

90. Edidin, M., Shrinking patches and slippery rafts: scales of domains in the plasma membrane. *Trends in Cell Biology* **2001,** 11, (12), 492-496.

91. Schuck, S.; Honsho, M.; Ekroos, K.; Shevchenko, A.; Simons, K., Resistance of cell membranes to different detergents. *Proceedings of the National Academy of Sciences of the United States of America* **2003,** 100, (10), 5795-5800.

92. Murase, K.; Hirako, Y.; Fujiwara, T.; Iino, R.; Owaribe, K.; Ritchie, K.; Kusumi, A., Single-molecule tracking/dragging revealed transient actin severing in the membrane skeleton as a mechanism for intercompartmental hop movement of membrane molecules. *Biophysical Journal* **2004,** 86, (1), 525A-525A.

93. Bartlett, P. F.; Mackay, I. R., The Oligodendroglial Cell - Biology and Immunology and Relationship to Multiple-Sclerosis. *Journal of Clinical & Laboratory Immunology* **1983,** 11, (1), 1-7.

94. Baron, W.; de Jonge, J. C.; de Vries, H.; Hoekstra, D., Perturbation of myelination by activation of distinct signaling pathways: An in vitro study in a myelinating culture derived from fetal rat brain. *Journal of Neuroscience Research* **2000,** 59, (1), 74-85.

95. Baumann, N.; Pham-Dinh, D., Biology of oligodendrocyte and myelin in the mammalian central nervous system. *Physiological Reviews* **2001,** 81, (2), 871-927.

96. DeBruin, L. S.; Haines, J. D.; Wellhauser, L. A.; Radeva, G.; Schonmann, V.; Bienzle, D.; Harauz, G., Developmental partitioning of myelin basic protein into membrane microdomains. *Journal of Neuroscience Research* **2005,** 80, (2), 211-225.

97. Taylor, C. M.; Coetzee, T.; Pfeiffer, S. E., Detergent-insoluble glycosphingolipid/cholesterol microdomains of the myelin membrane. *Journal of Neurochemistry* **2002,** 81, (5), 993-1004.

98. Heerklotz, H., Triton promotes domain formation in lipid raft mixt *Biophysical Journal* **2002,** 83, (5), 2693-2701.

99. Heerklotz, H.; Szadkowska, H.; Anderson, T.; Seelig, J., The sensitivity of lipid domains to small perturbations demonstrated by the effect of triton. *Journal of Molecular Biology* **2003,** 329, (4), 793-799.

100. de Almeida, R. F. M.; Fedorov, A.; Prieto, M., Sphingomyelin/phosphatidylcholine/cholesterol phase diagram: Boundaries and composition of lipid rafts. *Biophysical Journal* **2003,** 85, (4), 2406-2416.

101. Skwarek, M., Recent controversy surrounding lipid rafts. *Archivum Immunologiae Et Therapiae Experimentalis* **2004,** 52, (6), 427-431.

102. Bacia, K.; Scherfeld, D.; Kahya, N.; Schwille, P., Fluorescence correlation spectroscopy relates rafts in model and native membranes. *Biophysical Journal* **2004,** 87, (2), 1034-1043.